

Discovery of a Potent, Orally Bioavailable PI4KIII β Inhibitor (UCB9608) Able To Significantly Prolong Allogeneic Organ Engraftment *in Vivo*

James Reuberson,^{*,†,‡,§} Helen Horsley,[†] Richard J. Franklin,[†] Daniel Ford,[†] Judi Neuss,[†] Daniel Brookings,[†] Qiuya Huang,[‡] Bart Vanderhoydonck,^{‡,||} Ling-Jie Gao,[‡] Mi-Yeon Jang,[‡] Piet Herdewijn,^{‡,§} Anant Ghawalkar,[§] Farnaz Fallah-Arani,[†] Adnan Khan,[†] Jamie Henshall,[†] Mark Jairaj,[†] Sarah Malcolm,[†] Eleanor Ward,[†] Lindsay Shuttleworth,[†] Yuan Lin,[‡] Shenggiao Li,[‡] Thierry Louat,[‡] Mark Waer,[‡] Jean Herman,[‡] Andrew Payne,[†] Tom Ceska,[†] Carl Doyle,[†] Will Pitt,^{†,§} Mark Calmiano,[†] Martin Augustin,[⊥] Stefan Steinbacher,[⊥] Alfred Lammens,[⊥] and Rodger Allen[†]

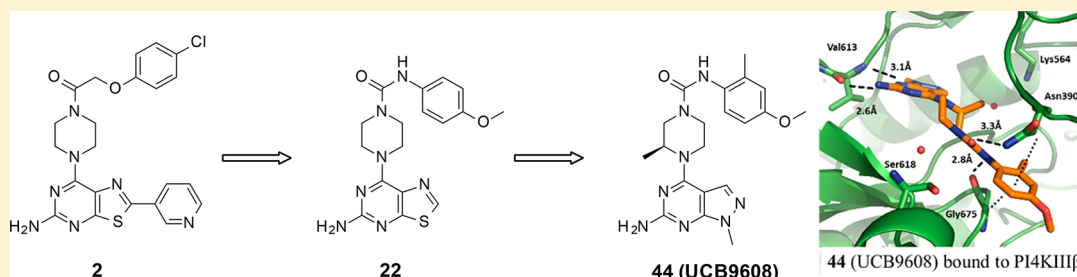
[†]UCB Pharma, 208 Bath Road, Slough, Berkshire SL1 3WE, United Kingdom

[‡]Interface Valorization Platform, KU Leuven, Campus St.-Rafaël, Blok I, 8°, Kapucijnenvoer 33 B 7001, 3000 Leuven, Belgium

[§]SAI Life Sciences Ltd, International Biotech Park, Hinjewadi, Pune 411 057, India

[⊥]Proteros Biostructures GmbH, Bunsenstrasse 7a, 82152 Martinsried, Germany

Supporting Information



ABSTRACT: The primary target of a novel series of immunosuppressive 7-piperazin-1-ylthiazolo[5,4-*d*]pyrimidin-5-amines was identified as the lipid kinase, PI4KIII β . Evaluation of the series highlighted their poor solubility and unwanted off-target activities. A medicinal chemistry strategy was put in place to optimize physicochemical properties within the series, while maintaining potency and improving selectivity over other lipid kinases. Compound **22** was initially identified and profiled *in vivo*, before further modifications led to the discovery of **44** (UCB9608), a vastly more soluble, selective compound with improved metabolic stability and excellent pharmacokinetic profile. A co-crystal structure of **44** with PI4KIII β was solved, confirming the binding mode of this class of inhibitor. The much-improved *in vivo* profile of **44** positions it as an ideal tool compound to further establish the link between PI4KIII β inhibition and prolonged allogeneic organ engraftment, and suppression of immune responses *in vivo*.

INTRODUCTION

The field of transplantation medicine has seen dramatic advances over the past century, with breakthroughs in management of immune responses and the development of genetically engineered animals for xenografting and the emerging use of organs from living donors.¹ In the United States alone, nearly 17,000 kidney, 6,700 liver, 2,600 heart, and 1,900 lung transplants are performed annually.² Successful management of immunosuppression, heralded by the discovery that corticosteroids³ could improve graft retention, led to the key discoveries of the 1980s, which were crucial to the further development of transplantation science. In particular, the discovery of cyclosporine A (CSA)⁴ and tacrolimus (Tac or FK506),⁵ cyclic peptides that had profound anti-calceinurin activity, was key. These peptidic calcineurin inhibitors (CNIs)

were found to inhibit T-cell activation, resulting in a strong immunosuppressive effect. Current immunosuppressive regimens promoting long-term graft survival use these CNIs in combination with steroids and myco-phenolate mofetil⁶ (MMF). Although reduced allograft rejection rates have been achieved, there are still risks associated with CNI therapies, including potential nephrotoxicity,⁷ and there remains a case for the discovery of alternative immunosuppressive agents^{8,9} to prevent allograft rejection.

In 2011, Jang et al.¹⁰ reported the discovery of a series of novel 7-piperazin-1-ylthiazolo[5,4-*d*]pyrimidin-5-amine analogues with a novel immunosuppressive effect (Figure 1).

Received: April 3, 2018

Published: June 28, 2018

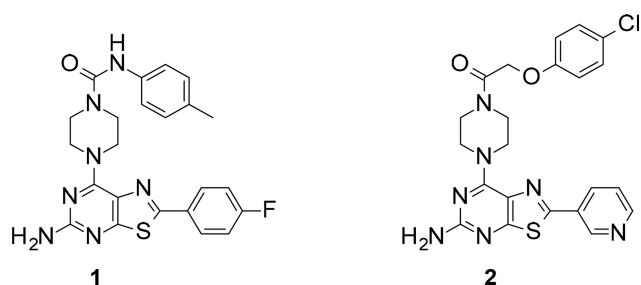


Figure 1. Previously described 7-piperazin-1-ylthiazolo[5,4-*d*]pyrimidin-5-amine analogues with immunosuppressive activity.

51 The compounds were shown to be potent in the human mixed
52 lymphocyte reaction (HuMLR) assay, often used as a surrogate
53 *in vitro* assay to predict the prevention of rejection *in vivo*
54 response, **2** appeared to prevent the rejection of a heterotopic
55 murine cardiac allograft from a C57BL/6 donor mouse to a
57 Balb/C H-2 recipient, confirming that compounds of this class
58 could suppress an allogeneic response *in vivo*.

59 ■ RESULTS AND DISCUSSION

60 With **2** as a series exemplar, commercial screening platforms
61 (Cerep¹⁴ and DiscoverX's KinomeScan¹⁵) were employed to
62 establish the primary target of these novel inhibitors. No
63 noticeable activity was recorded against the Cerep panel;
64 however, kinase profiling suggested that the most likely target
65 of **2** was a member of the lipid kinase family, PI4KIII β .¹⁶
66 PI4KIII β is a phosphatidylinositol kinase widely expressed in
67 mammalian cells, playing an essential role in membrane
68 trafficking and signal transduction.¹⁷ Sub-families include the
69 PI3KC1, C2, and C3 families and the PI4K class II and III
70 families. The PI4K class II's are further divided (PI4KII α and
71 PI4KII β), as are the PI4K class III's (PI4KIII α and
72 PI4KIII β).¹⁸ PI4K's are essential for the synthesis of PI4P
73 (phosphatidylinositol 4-phosphate), the most abundant

phosphoinositide in eukaryotic cells,¹⁹ and play critical roles
74 in a number of pathological processes, including mediating the
75 replication of a number of viruses,²⁰ and in the development of
76 the parasite responsible for malaria.²¹ PI4KIII β is also
77 understood to play a key role in cell compartmentalization
78 within the Golgi²² and the trans-Golgi network (TGN). Here
79 it is recruited by the Golgi resident ACBD3 protein²³ and plays
80 a role in lysosomal²⁴ and lipid transport functions.²⁵ There is
81 significant interest in targeting PI4KIII α and PI4KIII β
82 isoforms, as both are hijacked by multiple viruses, which
83 facilitate their entry to target cells and their subsequent
84 replication.^{26–29} At the time of discovery of **2**, there were
85 limited examples of PI4KIII β inhibitors in the literature. PIK93
86 (**3**, Figure 2), originally developed to target PI3KC1
87 isoforms,³⁰ showed concurrent activity against both PI4KIII α
88 (IC₅₀ = 1.1 μ M) and PI4KIII β (IC₅₀ = 0.019 μ M). Recently
89 the structure of this pan-lipid kinase, co-crystallized with
90 PI4KIII β , was published.^{31,32} Furthermore, analogues of PIK-
91 93, such as **4**, have been disclosed with improved PI4KIII β ³³
92 selectivity, with **5**, **6**, and **7** emerging as further examples of this
93 class of PI4KIII β inhibitor, showing anti-hepatitis C^{34,35} and
94 anti-human rhinovirus³⁶ activity, respectively. The selective
95 PI4KIII β inhibitor **8** has also been designed to probe the role
96 of phosphatidylinositol signaling in cancer cell prolifera-
97 tion.^{37,38} A somewhat structurally related chemotype,
98 exemplified by **9**, was identified as having anti-polio virus
99 activity,³⁹ and PI4KIII β was established as the likely driver for
100 this observed effect. The syntheses⁴⁰ of related analogues such
101 as **10** and the structurally differentiated **11** have also been
102 disclosed,⁴¹ and they are shown to be potent and selective
103 PI4KIII β inhibitors with anti-viral activity established against
104 human rhinovirus and the polio virus. Further core
105 modification of **9** has also been successful in delivering potent
106 inhibitors of PI4KIII β , with excellent selectivity profiles.^{42–45}
107 Rationally designed inhibitors such as **12**, were shown to be
108 broad spectrum antiviral agents with excellent selectivity for
109 PI4KIII β over other lipid kinases, with the structure of several
110

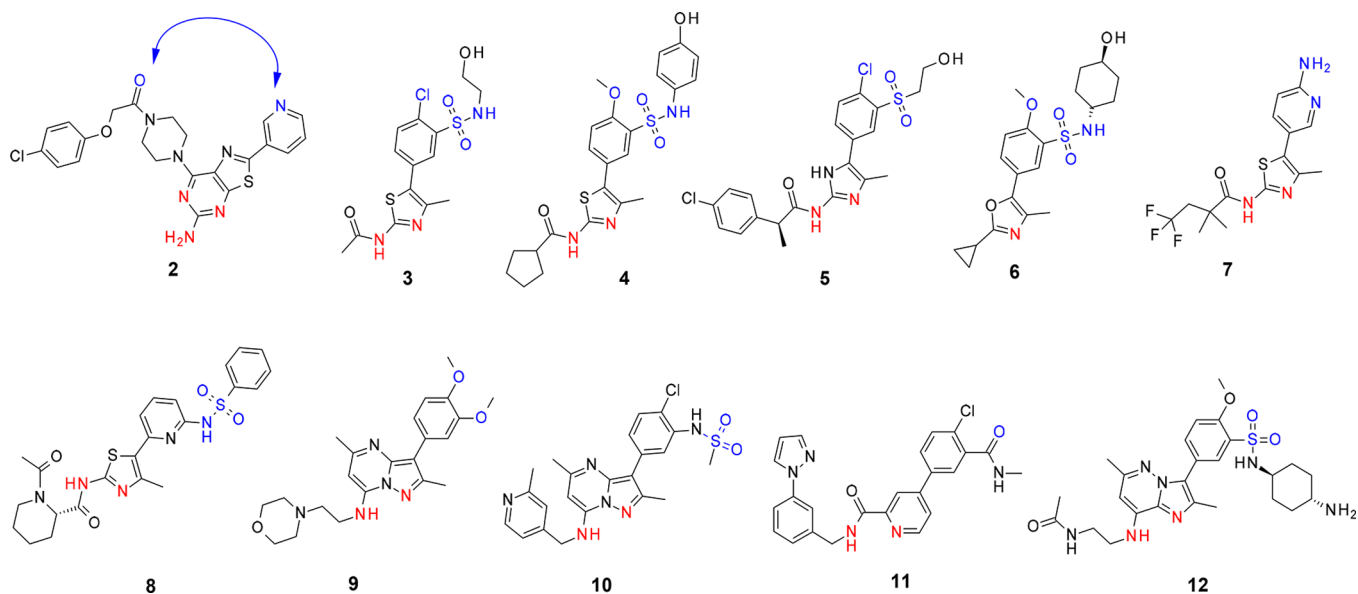
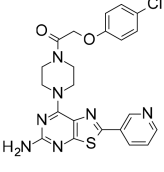
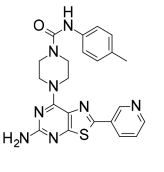
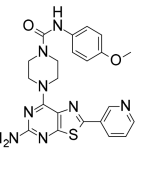
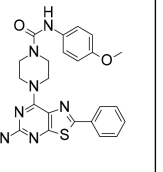
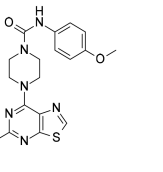


Figure 2. Compound **2** in a proposed alignment with exemplar structures of PI4KIII β inhibitors from literature (**3–12**). The nitrogen atoms postulated to form the key mono or bidentate interaction with the kinase hinge region are shown in red. Atoms in blue, are likely to be involved in a second critical interaction with the catalytic lysine residue of PI4KIII β . It was plausible **2** could adopt multiple binding modes with the piperazine and 3-pyridyl groups "flipping" to make a putative interaction with the lysine residue (as highlighted by the blue arrow).

Table 1. Early *in Vitro* Profiling of 7-Piperazin-1-ylthiazolo[5,4-*d*]pyrimidin-5-amine Series

Compound:	2	13	14	15	22
					
PI4KIII β IC ₅₀ (nM) ^a	10	19	2	11	51
Hu MLR IC ₅₀ (nM) ^a	16	5	4	32	53
MLM CL _{int} (μ l.min ⁻¹ .mg ⁻¹)	133	72	87	20	15
HLM CL _{int} (μ l.min ⁻¹ .mg ⁻¹)	34	32	35	13	21
hERG IC ₅₀ (μ M)	- ^c	2.0	2.2	1.7	28
CYP3A4 IC ₅₀ (μ M)	- ^c	0.9	1.6	>20 ^c	>20
LogD (pH7.4)	- ^c	3.42	3.06	- ^c	1.85
Solubility (μ M) ^b	- ^c	9	32	6	85

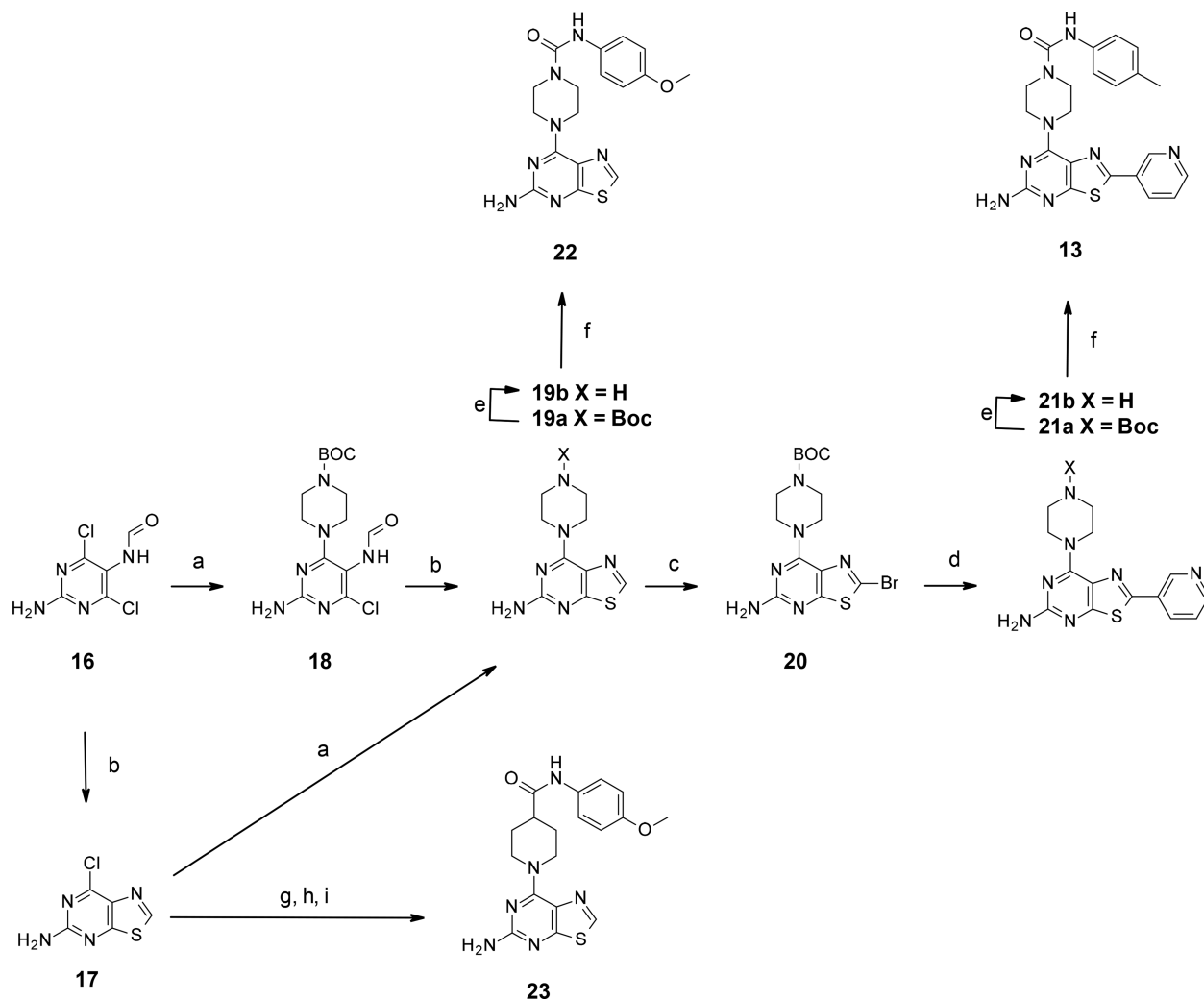
^aIC₅₀ values are reported as means of values from at least two determinations. ^bKinetic solubility measured from 10 mM DMSO stock at pH 7.4. ^cPoor solubility means data were unobtainable or should be treated with caution.

111 inhibitors of this type bound to the complex of PI4KIII β /
112 wtRab11 disclosed.

113 Compounds 2–12 all share a putative hydrogen-bonding
114 interaction with the hinge region of PI4KIII β . A second
115 interaction to a catalytic lysine is also present in compounds
116 3–12; however, it was not clear if 2 was deriving its activity by
117 making the same interaction (Figure 2). To this end, we
118 sought to confirm the binding mode of these novel inhibitors,
119 establish the link between PI4KIII β inhibition and impaired
120 immune cell function, and evaluate if PI4KIII β inhibitors from
121 this unique series had the potential to become part of a new
122 CNI sparing immunosuppressive regimen for the prevention of
123 the rejection of solid organ allografts. The HuMLR continued
124 to be used in the absence of any cellular assay where PI4KIII β
125 target engagement could be directly measured. As discussed
126 previously, the HuMLR is a phenotypic assay, used as a
127 predictor of the classical immune response (i.e., “self”
128 responding to “non-self”). To validate the effectiveness of
129 the HuMLR as a surrogate cellular assay for assessing PI4KIII β
130 inhibitors as immunosuppressive agents, the IC₅₀'s of a
131 selection of differentiated PI4KIII β chemotypes from Figure
132 2 were generated. PIK-93 (3) was found to inhibit the HuMLR
133 with IC₅₀ = 28 nM; however, as discussed previously, PIK-93 is
134 a pan-lipid kinase inhibitor, designed to primarily target the
135 PI3K's. The more selective analogue 5 was also found to
136 inhibit the HuMLR, with IC₅₀ = 71 nM, in line with its
137 reported PI4KIII β activity.⁴⁶ Compound 9 showed modest
138 activity in the HuMLR (IC₅₀ = 2 μ M), likely due to its poor
139 cell permeability, while 10 inhibited the HuMLR with IC₅₀ = 8
140 nM. Finally, 11 was found to have an IC₅₀ against the HuMLR
141 of 18 nM. Both 10 and 11 were described as being selective
142 inhibitors of PI4KIII β kinase,⁴⁷ adding weight to the notion
143 that PI4KIII β inhibition was responsible for the reduced
144 HuMLR response of this structurally diverse set of inhibitors
145 (2, 5, 10, and 11). As a means of prioritizing compounds for

146 evaluation as potential immunosuppressive agents *in vivo*, the
147 HuMLR was deemed to be a simplistic and robust assay to
148 continue to screen against, although whether all PI4KIII β
149 inhibitor chemotypes could replicate the effect seen with
150 compound 2 *in vivo* remained to be confirmed. A more in-
151 depth evaluation of analogues of 1 and 2, some of which were
152 detailed in the previous KUL publication,¹⁰ was now
153 undertaken at UCB. This included *in vitro* safety profiling
154 (drug–drug interaction (DDI) risk and cardiovascular safety
155 (CVS) risk), *in vitro* metabolic stability in mouse liver
156 microsomes (MLMs) and human liver microsomes (HLMs),
157 and measurement of physicochemical parameters such as
158 LogD and solubility. Of the many compounds profiled, 2 and
159 13 stood out as potent examples of amide- and urea-capped 7-
160 piperazin-1-ylthiazolo[5,4-*d*]pyrimidin-5-amine analogues re-
161 spectively (Table 1).

162 Although both compounds showed promising potency, the
163 solubility of 2 and 13 was poor, and CL_{int} in HLM and MLM
164 was moderate to high. Compound 13 was also found to inhibit
165 the hERG channel with IC₅₀ = 2 μ M (automated patch-
166 clamping (Q-Patch)), indicative of a potential CVS risk⁴⁸ as
167 well as CYP3A4, with IC₅₀ = 0.9 μ M, indicative of a potential
168 DDI risk.⁴⁹ It was not possible to profile 2 in these assays due
169 to its poor solubility. Urea analogue 14 showed improved
170 PI4KIII β and HuMLR potency but remained a strong inhibitor
171 of both hERG and CYP3A4, with CL_{int} in HLM and MLM
172 remaining high. The phenyl analogue 15 maintained accept-
173 able activity, suggesting the 3-pyridyl nitrogen in 14 was not
174 critical for maintaining PI4KIII β activity. Encouragingly, 15
175 appeared to be more stable (compared to 14) in HLM and
176 MLM, while CYP3A4 inhibition appeared significantly
177 reduced, although it is noted that the poor solubility of this
178 compound meant that these data should be treated with
179 caution.

Scheme 1. Synthesis of Compounds 13, 22, and 23^a

^aReagents and conditions: (a) Boc-piperazine, 1,4 dioxane, DIPEA, 1 h, 55 °C, quant; (b) Lawesson's reagent, 1,4 dioxane, 0.5 h, 65 °C, 93%; (c) NBS, DMF, 3 h, 55%; (d) 3-(Et₂B)-pyridine, Na₂CO₃(aq), Pd(0)(PPh₃)₄, DME, 150 °C, CEM microwave, 0.5 h, 45%; (e) 4 N HCl in 1,4-dioxane, DCM, 1–16 h, 72–100%; (f) isocyanate, DIPEA or Et₃N, DCM or DMF, 4 h, 20–95%; (g) ethyl isonipecotat, DIPEA, 1,4-dioxane, 12 h, 70 °C, 50%; (h) 10% NaOH, THF/MeOH (5:1), 6 h, quant; (i) *p*-anisidine, HOBT·H₂O, EDCI, DIPEA 14 h, 81%.

180 It could not be ruled out that removal of the pyridyl
181 nitrogen, a potential heme binding element could be playing a
182 significant part in the improved *in vitro* ADME profile observed
183 with 15. The route previously¹⁰ utilized to access compounds 2
184 and 13 was modified to allow for exploration of the 2-position
185 of the thiazolo[5,4-*d*]pyrimidine-5-amine core. The Boc-
186 protected 2*H*-thiazolo[5,4-*d*]pyrimidine-5-amine 19a was
187 synthesized from commercial 16 in 2 interchangeable steps
188 according to Scheme 1. Bromination of intermediate 19a using
189 NBS in 1,4-dioxane yielded 20, a flexible intermediate suitable
190 for the exploration of the 2-position via a range of coupling
191 methodologies. To validate the route, compound 13 was
192 resynthesized using this new approach, coupling diethyl(3-
193 pyridyl) borane with 20. Deprotection of 21a then subsequent
194 capping with commercial 4-methylphenyl isocyanate gave 13
195 in good yields. It was intended that with 20 in hand, a SAR
196 exploration of the 2-position could be initiated with the aim of
197 identifying potent, soluble, and more metabolically stable
198 analogues of 14 and 15 that were free of hERG and CYP
199 liabilities. Interestingly, upon testing the unsubstituted 2*H*-
200 thiazolo[5,4-*d*]pyrimidine-5-amine analogue 22, an acceptable

level of PI4KIIIβ and HuMLR activity could be maintained. 201
Indeed, with this ring excised, LogD was reduced, and 202
subsequently MLM and HLM CL_{int} were improved. A modest 203
improvement in kinetic solubility was also noted, and 204
inhibition of both CYP3A4 and hERG (although not 205
completely ablated) was much reduced (Table 1). At this 206
juncture, both 13 and 22 were chosen for kinase selectivity 207
profiling. A set of 250 diverse kinases⁵⁰ were screened at a 208
concentration of 10 μM. No activity was noted against any 209
tested kinase aside from a handful of lipid kinase isoforms. 210
Concentration responses (IC₅₀) were obtained against the 12 211
available lipid kinases,⁵¹ and a selectivity profile for 13 and 22 212
was generated (Figure 3). It appeared that 22 was 15-fold 213
selective for PI4KIIIβ over PI3KC2γ,⁵² 50-fold over PI3KC2α, 214
and 120-fold over PI3KC2β. Compound 13, with the 215
appended 3-pyridyl ring, appeared to be more selective for 216
PI4KIIIβ over the PI3KC2 family of kinases in comparison. 217
The impact of this modest PI3KC2 inhibition was not clear, as 218
the role of these kinases in disease, and their subsequent utility 219
as therapeutic targets,⁵³ is still being explored. Encouragingly, 220
both 13 and 22 showed no activity against the other PI4K 221

X fold selectivity for PI4KIII β of **13** and **22** against members of the lipid kinase family

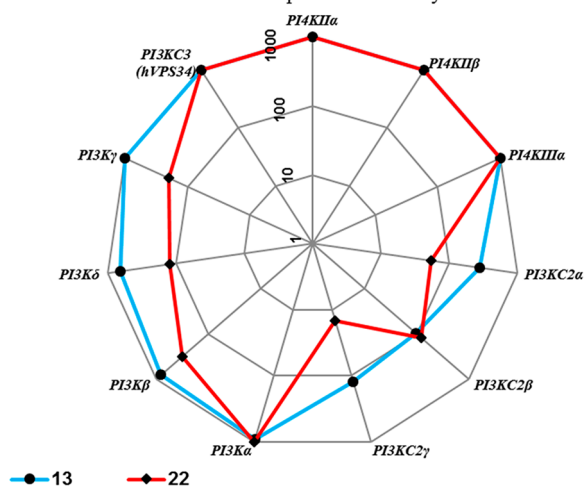


Figure 3. Radial plot of lipid kinase selectivity of **13** and **22** for PI4KIII β over the other 11 lipid kinase family members tested.

22 isoforms and maintained good selectivity (>100-fold) over the class 1 PI3K α , β , γ , and δ isoforms (Figure 3).

224 Compound **22** was chosen on the basis of its *in vitro* profile to evaluate PI4KIII β inhibition in murine models of T-cell mediated immune response. The blood concentration vs time profile in male Balb/C mice following oral administration at 10, 30, and 100 mpk was determined for **22**, prior to evaluation in a mouse model of anti-CD3-mediated T-cell activation.⁵⁴ Exposure appeared to increase in proportion to dose; however, there was significant inter-individual variation in exposure observed, likely influenced by the poor solubility of **22** leading to highly variable oral absorption across the doses tested. C_{max}

(free) was achieved at around 1 h at all doses, and for the 100 mpk dose, it was between 10- and 30-fold over the HuMLR IC_{50} .

As seen in Figure 4, **22** significantly inhibited IFN γ release compared to vehicle treated animals in a dose-dependent manner, indicative of **22** having a strong inhibitory effect on T-cell activation. Subsequent evaluation of **22** in a longer term oxazolone (OXA)-induced T-cell-dependent model of antibody response⁵⁵ (Figure 5) showed that **22** could also significantly inhibit IgG1 production at a dose of 100 mpk (p.o.). With **22** able to inhibit a range of T-cell-mediated antibody responses *in vivo*, it was left to evaluate if the modified urea **22** remained efficacious in the murine model of cardiac allograft rejection¹⁰ previously described by the team at KUL. Balb/C mice carrying a heterotopically transplanted heart from a C57B6 donor were treated once daily with 100 mpk of **22**, and long-term graft survival rates of ~50%, when compared to vehicle⁵⁶ alone, could be achieved. Significantly animals treated with **22** continued to maintain their grafts after treatment withdrawal, differentiating them from CSA treated animals (Figure 5) where rejection occurred days after treatment withdrawal.

The majority of graft rejection seen with **22** took place during a time critical period post-surgery, when risk of acute rejection is at its highest.⁵⁷ Given the delicate nature of the surgery involved, obtaining multiple PK samples during this critical time was challenging, and establishing the relationship between free drug levels and long-term graft survival was problematic. With the high inter-individual variability in exposure following oral administration of **22**, possibly driven by poor solubility (see Figure 4), there remained uncertainty as to how much drug each engrafted animal was receiving, during the critical post-surgery window. To establish more accurately

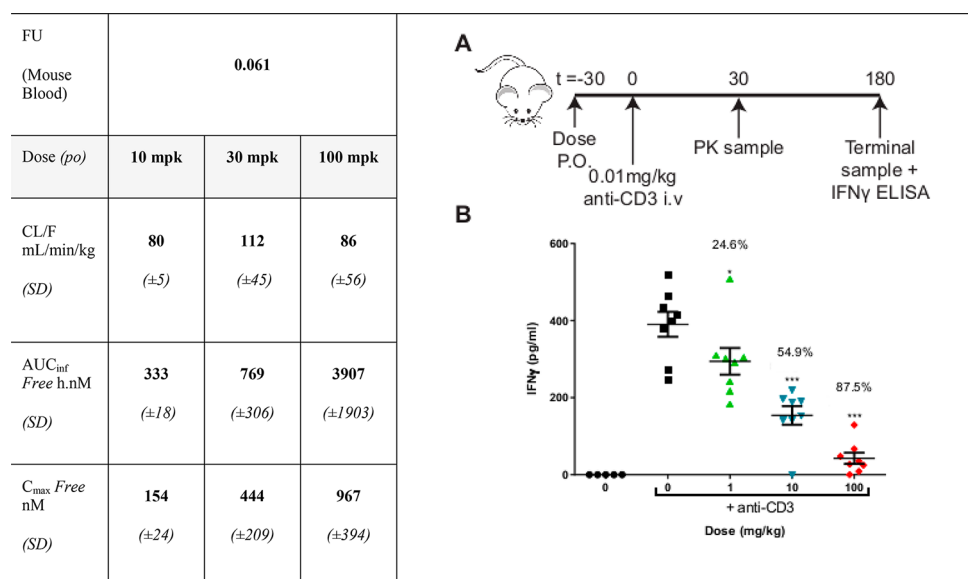


Figure 4. Oral PK parameters were determined in male Balb/C mice, $n = 3$, at the specified dose, with crystalline **22** given as a homogeneous suspension in vehicle (0.1% (w/v) Tween 80, 0.1% (w/v) silicone antifoam in 1% (w/v) methylcellulose (400 cps) in water). (A) Time course (in minutes) for assessing the inhibition of anti-CD3-induced T-cell activation of IFN γ release by **22**. (B) Measured levels of IFN γ release (pg/mL) for negative control, positive control (vehicle (0.1% (w/v) Tween 80, 0.1% (w/v) silicone antifoam in 1% (w/v) methylcellulose (400 cps) in water)), 1, 10, and 100 mpk of **22** (all groups $n = 8$). % Inhibitions refer to the mean (\pm SEM). * $P < 0.05$ compared to positive control by Dunnett's multiple comparison test. *** $P < 0.001$ compared to positive control by Dunnett's multiple comparison test. PK samples were taken 1 h after dosing with **22** to coincide with C_{max} and confirmed that exposures achieved in the experiment were in line with those achieved during the PK study.

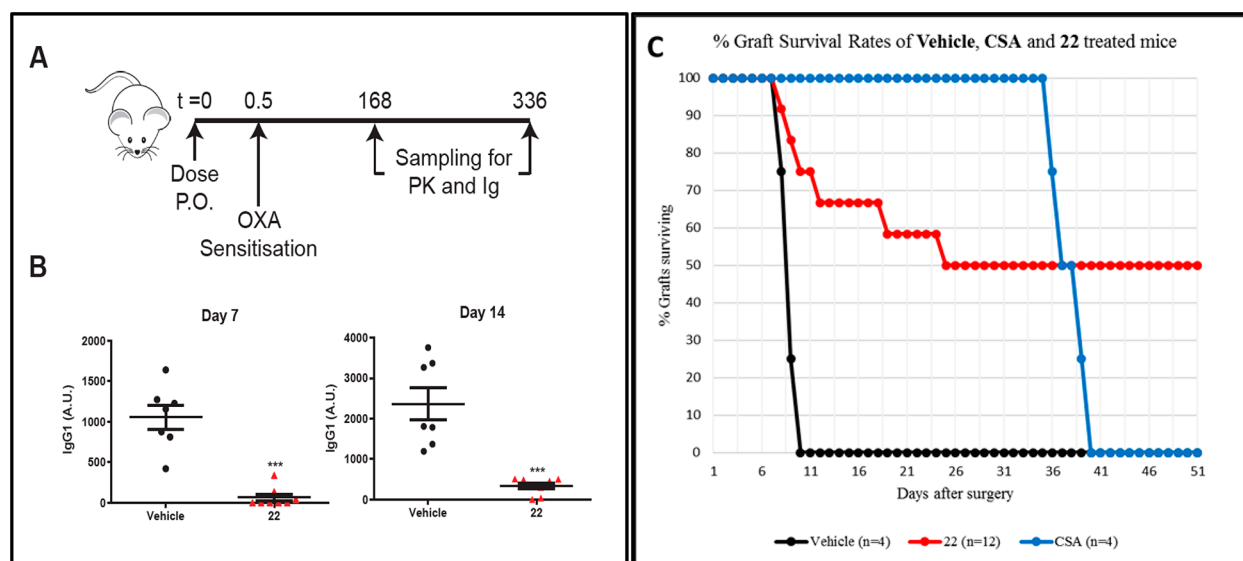
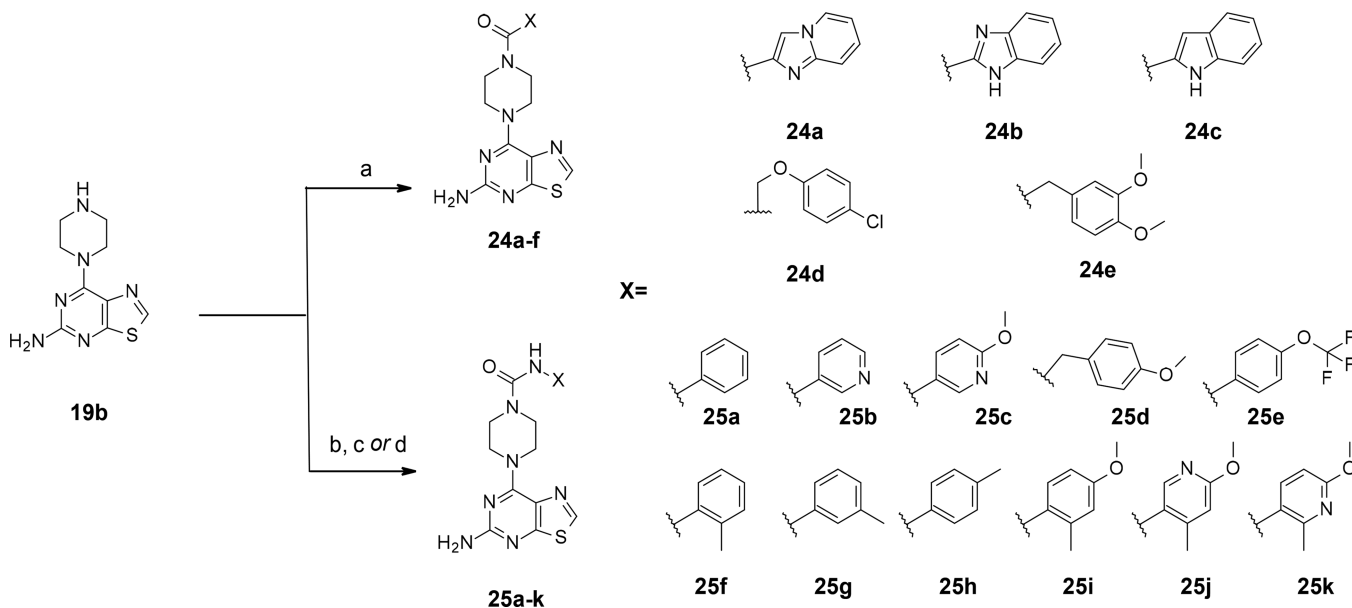


Figure 5. (A) Time course (in hours) for assessing the inhibition of OXA induced IgG1 release by 22 ($n = 8$). (B) Measured IgG1 levels after daily dosing of vehicle (0.1% (w/v) Tween 80, 0.1% (w/v) silicone antifoam in 1% (w/v) methylcellulose (400 cps) in water) and 22 (100 mpk of crystalline 22 as a homogeneous suspension in vehicle), measured at day 7 and day 14 compared to vehicle control (arbitrary units, AU). *** $P < 0.001$ compared to positive control by Dunnett's multiple comparison test. (C) Comparison of survival rates for engrafted mice treated with vehicle (0.1% (w/v) Tween 80, 0.1% (w/v) silicone antifoam in 1% (w/v) methylcellulose (400 cps) in water), CSA (40 mpk as a solution in vehicle), and 22 (100 mpk of crystalline 22 as a homogeneous suspension in vehicle). Animals were dosed via oral gavage once a day for 28 days, or until a transplanted graft had ceased beating, indicative of rejection. Graft survival is defined as a strongly beating heart (as confirmed by visual inspection and palpitation).

Scheme 2. Synthesis of Amide, Aryl, and Heteroaryl Urea Analogues of 22^a



^aReagents and conditions: (a) acid, HATU, DIPEA, DMF, 12 h, 50–90%; (b) aryl isocyanate, DIPEA or Et₃N, DCM or DMF, 4 h, 20–95%; (c) aryl-amine, CDI, DMF, DIPEA, 4 h, 20–95%; (d) aryl-amine, PhOCOCl, pyridine, THF then DIPEA, DMSO, 3 h, 60 °C, 50 and 90%.

267 the link between PI4KIII β inhibition and successful engraftment in this and other transplantation models, a tool 268 compound from this series, with a much improved and 269 reproducible PK profile, was required. Further SAR exploration 270 was undertaken to improve potency and solubility while 271 establishing if compounds such as 22, carrying an embedded 272 electron-rich anilino-urea, posed any toxicity liability. Many 273 aryl ureas are found in marketed kinase inhibitors,⁵⁸ but there 274 remains a potential for the metabolically triggered release of 275

electron-rich anilines, raising a potential genotoxicity⁵⁹ or liver 276 toxicity risk, as seen with acetaminophen.⁶⁰ Considerable effort 277 was spent seeking more soluble, non-urea equivalents of 22. 278 First, the piperazine amide equivalent 23 was made as detailed 279 in Scheme 1. 280

Swapping out the piperazine urea nitrogen for an sp³ carbon 281 was significantly detrimental to PI4KIII β activity (IC₅₀ > 6 282 μ M). Subsequently focus turned to making piperazine amides. 283 Libraries of aliphatic and aromatic amides were made; 284

Table 2. SAR of Non-urea Analogues of 22

Cpd	24a	24b	24c	24d	24e
PI4KIIIβ IC ₅₀ (nM) ^a	946	6138	>10000	216	5743
HuMLR IC ₅₀ (nM) ^a	8795	>10000	>10000	635	>10000
LogD (pH7.4)	1.58	2.54	2.84	2.68	1.50
Solubility ^b (μM)	>350	38	14	13	>350

^aIC₅₀ values are reported as means of values from at least two determinations. ^bKinetic solubility measured from DMSO stock at pH 7.4.

Table 3. SAR of Aryl and Heteroaryl Urea Analogues of 22

Cpd	25a	25b	25c	25d	25e	25f	25g	25h	25i	25j	25k
PI4KIIIβ IC ₅₀ (nM) ^a	517	3387	611	1946	548	114	312	145	9	414	173
Hu MLR IC ₅₀ (nM) ^a	380	>5000	424	1764	331	150	115	85	35	656	195
Solubility (μM) ^b	178	>350	293	33	12	33	34	21	33	>350	207
LogD (pH 7.4)	2.21	1.46	1.79	2.22	3.39	2.12	2.81	2.55	2.03	1.66	1.65

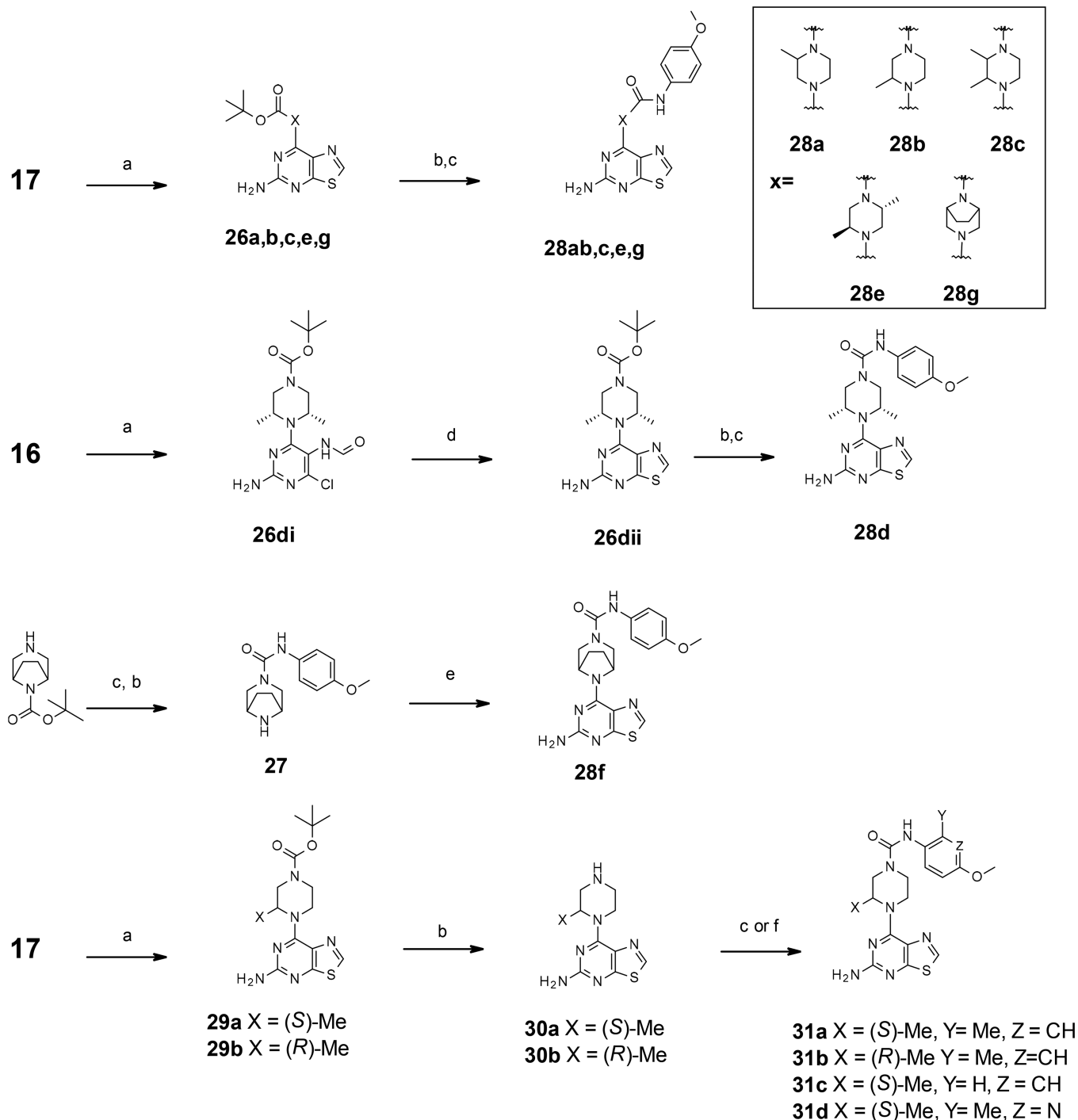
^aIC₅₀ values are reported as means of values from at least two determinations. ^bKinetic solubility measured from DMSO stock at pH 7.4.

285 however, all but a few showed potencies in the sub-μM range,
286 with the synthesis of key examples detailed in Scheme 2. These
287 included heterocyclic amides such as the imidazo-pyridine 24a,
288 that also showed a modest improvement in solubility. Attempts
289 to improve potency by adding back the hydrogen bond donor
290 of 22, were unsuccessful, with benzimidazole 24b and indole
291 24c significantly less active (Table 2). The only amide
292 analogue of 22 that appeared to have any significant potency
293 was 24d, an analogue of the original lead 2. The IC₅₀ against
294 PI4KIIIβ was 216 nM but solubility was significantly worse
295 than 22, with subsequent analogues continuing to suffer from
296 modest potency, poor solubility, and metabolic instability. The
297 phenyl acetamide 24e, where the NH of 22 is swapped for a
298 methylene, was significantly less active, adding to the evidence
299 supporting the importance of the urea CO and NH in 22
300 maintaining activity.

301 Without a published PI4KIIIβ crystal structure (at this time)
302 to aid design, further efforts to seek urea replacements were
303 halted. The concern around the inherent risk of genotoxicity
304 associated with embedded electron-rich anilines prompted the
305 profiling of 22 in a three-strain bacterial mini-AMES⁶¹ test. It
306 concluded that 22 was non-mutagenic at the top concen-
307 trations tested, with and without metabolic activation. There
308 was, however, literature evidence to suggest 4-methoxy aniline

(*p*-anisidine) was a likely genotoxic liability,⁶² although 309
metabolite profiling of 22 concluded no liberation of 4- 310
methoxy aniline in the presence of isolated human liver 311
microsomes.⁶³ A wide range of alternative urea analogues were 312
synthesized to explore SAR, drive potency, and improve 313
solubility, with key examples detailed in Table 3. Unsubstituted 314
aniline urea 25a was significantly less active, as was the 3- 315
pyridyl urea, 25b, although kinetic solubility was improved. 316
Potency could be returned to 25b, by making the methoxy- 317
pyridine analogue 25c, which maintained modest potency, 318
although 10-fold less active than 22. Homologation to the 319
benzyl urea 25d reduced activity, with the more electron- 320
withdrawing 4-OCF₃ analogue, 25e, 10-fold less active than 22. 321
A simple methyl scan of the aryl urea (25f–h) showed a slight 322
preference for *ortho* or *para* substitution over *meta*, with all 323
three compounds appearing less active than 22 and 324
significantly less soluble. 325

The observation that an *ortho*-methyl group was tolerated in 326
25f was exploited, and 25i, the 2-methyl-4-methoxyanilino 327
urea, was found to have IC₅₀ = 9 nM against PI4KIIIβ, with 328
activity maintained in the HuMLR. Solubility was poor, 329
although it could be improved by making pyridine analogues 330
25j and 25k. Again, however, this came at the cost of potency, 331
with 25k the most active, with IC₅₀ ≈ 200 nM in the HuMLR. 332

Scheme 3. Synthesis of Substituted Piperazine Analogues^a

^aReagents and conditions: (a) substituted Boc-piperazine, DIPEA, 1,4-dioxane, 55–100 °C, 12–100 h, 6–80%; (b) TFA or HCl in 1,4-dioxane, rt, 2–24 h, 80–100%; (c) isocyanate, DIPEA, DCM or DMF, rt, 10–24 h, 40–80%; (d) Lawesson's reagent, THF, 70 °C, 3 h, quant.; (e) intermediate **17**, DIPEA, 1,4-dioxane, 100 °C, 100 h, 20%; (f) 6-MeO-2-Me-pyridin-3-amine, phenyl chloroformate, pyridine, THF, 0 °C, then addition to **30b** in DMSO with DIPEA, 60 °C, 3 h, 55%.

333 Further efforts to solubilize **25i** through aryl substitution, aryl
334 ring modification or addition of solubilizing groups to the
335 critical methyl or methoxy substituents (data not shown) failed
336 to give the balance of potency and solubility required. Focus
337 next shifted to reducing the planar nature of the compounds by
338 inducing a twist to the piperazine linker. It is known that by
339 reducing "flatness" or through the introduction of more three-
340 dimensional structure, the solubility of drug like molecules⁶⁴

can be significantly improved. Thus, a broad range of 341
monoprotected substituted piperazines were identified with 342
the synthesis of key analogues of **22**, detailed in Scheme 3. 343 s3
When a methyl was introduced adjacent to the urea linker 344
(**28a**), solubility was enhanced, but potency impacted. When 345
the methyl was added adjacent to the piperazine nitrogen 346
linking to the hinge binding group (**28b**), both primary and 347
cellular potency as well as kinetic solubility were much 348

Table 4. SAR of Substituted Piperazine Urea Analogues

Cpd	28a	28b	28c	28d	28e	28f	28g	31a	31b	31c	31d
PI4KIII β IC ₅₀ (nM) ^a	1500	18	2583	1412	275	981	2577	4	316	8	20
Hu MLR IC ₅₀ (nM) ^a	>10000	23	2712	543	381	635	1768	8	472	31	60
Kinetic Solubility (μ M) ^b	>350	>350	>350	83	88	>350	>350	160	170	>350	>350
Solubility -TD (μ M) ^c	-	-	-	-	-	-	-	3	-	30	362
hERG IC ₅₀ (μ M)	-	-	-	-	-	-	-	-	-	17	>30
CYP3A4 IC ₅₀ (μ M)	-	-	-	-	-	-	-	>20 ^d	-	>20	>20

^aIC₅₀ values are reported as means of values from at least two determinations. ^bKinetic solubility measured from DMSO stock at pH 7.4. ^cThermodynamic solubility (TD) measured from solid stock at pH 7.4. ^dFigure should be treated with caution due to low solubility.

improved relative to those of **22**. A further set of dimethylated and bridged piperazine linkers were synthesized (**28c–28g**), although none combined the potency and solubility improvements seen with **28b** (Table 4). Through use of the respective chiral Boc-methyl piperazines, building blocks **30a** and **30b** were synthesized to establish if there was any enantiomeric preference. Capping was then undertaken with the most potent urea to date, derived from 2-methyl-4-methoxy aniline. As can be seen in Table 4, there was a clear preference for the (*S*) enantiomer over the (*R*), with **31a** becoming the most potent analogue of **22** made to date.

Although **31a** appeared to show a modest improvement in kinetic solubility, when thermodynamic solubility⁶⁵ was measured there was no apparent difference in the solubility of **22** and **31a**. **31c** was made, the direct analogue of **22** bearing a single chiral methyl on the piperazine, and maintained single-digit nM potency with improved thermodynamic solubility compared to **22**.

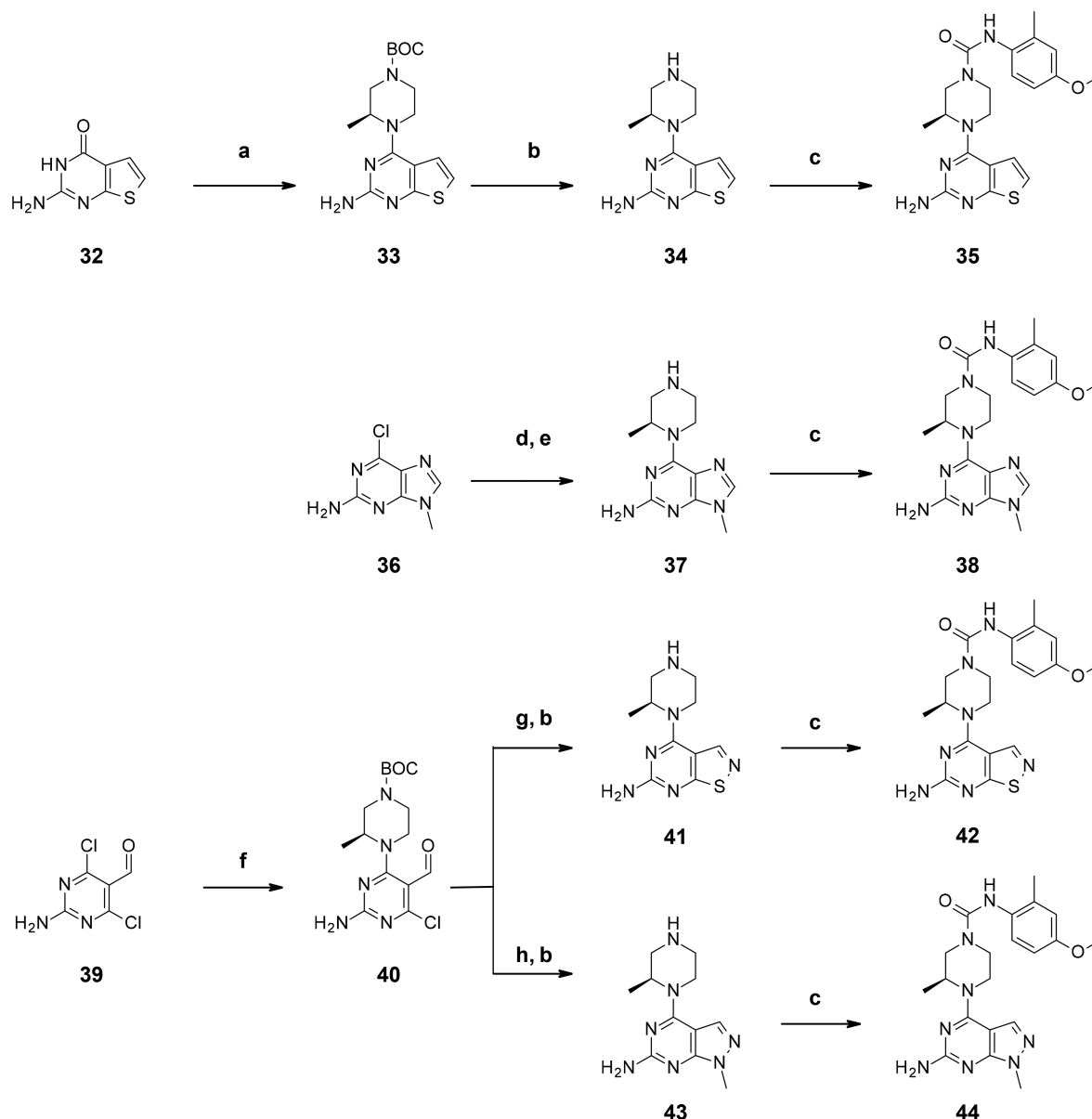
The pyridyl analogue **31d** showed a 5-fold drop off in PI4KIII β activity but was still more potent than **22** and exhibited excellent thermodynamic solubility. There was no CYP3A4 inhibition observed with any (*S*) methyl piperazine analogue tested, and pyridyl urea **31d** was clean in hERG. The more lipophilic **31c**, however, did exhibit a stronger hERG signal than **22**, but not enough to warrant concerns at this stage.

Finally, in a bid to further improve potency and solubility within the series, the 5-membered ring adjacent to the hinge-binding aminopyrimidine was investigated. Keeping the most potent piperazine urea combinations identified so far, analogues of **31a** were synthesized as detailed in Scheme 4. Deletion of the nitrogen of the thiazole ring to give the fused

thiophene **35** gave a potent analogue, but thermodynamic solubility was negligible, and the hERG signal had further increased as LogD increased. Swapping the sulfur of **31a** for an NMe group in purine analogue **38** (Scheme 4) gave a sub-10 nM PI4KIII β inhibitor, with HuMLR potency in line with that of **22**. Thermodynamic solubility was much improved with this hinge-binding heterocycle, and no hERG or CYP3A4 inhibition was observed.

The isothiazole **43** was also sub-10 nM against PI4KIII β , although a drop-off in the HuMLR was again noted. Thermodynamic solubility was modest, but as with **35**, a significant increase in the hERG signal was noted, although no CYP3A4 inhibition was present. Finally, the pyrazole analogue **44** (UCB9608) was synthesized and gave a good balance of potency and solubility, with no hERG or CYP flags, as shown in Table 5. Compounds **31c**, **38**, and **44** were chosen to be further evaluated *in vivo*. Prior to establishing mouse PK parameters, MLM and HLM stability was assessed. The addition of the chiral methyl piperazine to **22** (giving **31c**) had increased LogD, and metabolic stability was modestly impacted. The modifications made to the hinge binding region of **38** and **44** lowered LogD, and both MLM and HLM stability improved relative to **31c**. The efflux ratio (ER: Caco-2) for **22** and **38** indicated that these compounds were substrates for efflux transporters, while **31c** and **44** had a lower ER, indicative of a reduced risk. Mouse PK was performed for the three compounds, and data are shown in Table 6.

All three more soluble compounds showed low volume of distribution and moderate to short half-lives. The higher LogD **31c**, had a higher CL_b, compared to other analogues, and so free drug levels following p.o. administration were no better than those seen with **22**, despite being well absorbed.

Scheme 4. Synthesis of Hinge Binder Analogues of 31a^a

^aReagents and conditions: (a) PyBOP, DBU, acetonitrile, Boc-piperazine, 60 °C, 72 h, 66%; (b) 4 N HCl in 1,4-dioxane, 1–8 h, quant.; (c) 4-MeO-2-Me-phenylisocyanate, DIPEA, DCM or DMF, rt 4–24 h, 50–80%; (d) Boc-piperazine, DIPEA, NMP, 110 °C, 72 h, 49%; (e) 4 M HCl in methanol, 4 h, quant.; (f) Boc-piperazine, DIPEA, 1,4 dioxane, 80 °C 4 h, 93.8%; (g) sulfur, NH₄OH, NMP, 90 °C 4 h, 79%; (h) MeNHNH₂, THF, reflux 4 h, 47%.

413 Compound 38 although having a slightly lower CL_b than 31c,
 414 had a comparable half-life, impacted by its low volume of
 415 distribution. The bioavailability was also lower, which was
 416 unexpected due to the improved solubility and reduced
 417 clearance and may have been due to reduced intestinal
 418 absorption, driven by active transport, in line with Caco-2 data.
 419 Compound 44 had very low CL_b, commensurate with its low
 420 CL_{int} in MLM, leading to a half-life of 1.4 h, with high
 421 bioavailability, and low inter-individual variability. With its
 422 vastly improved oral PK profile in comparison to 22, the
 423 pyrazolopyrimidine 44 appeared to be an excellent *in vivo* tool
 424 compound. AMES MPF⁶⁶ screening of 44 showed no flags,
 425 and metabolic profiling in isolated human microsomes⁶⁷ again
 426 showed no evidence of urea hydrolysis or aniline-derived

metabolites. The embedded 2-methyl-4-methoxy aniline was 427
 also assessed in AMES MPF and appeared free of risk.⁶⁸ 428

Kinome-wide screening⁵⁰ of 44 was undertaken, and of the 429
 250 kinases tested at 10 μM, only the PI4KIIIβ and PI3KC2 α, 430
 β, and γ lipid kinases were inhibited. The selectivity profile of 431
 44 for PI4KIIIβ over the 11 available lipid kinases confirmed 432
 that 44 had a much improved selectivity profile⁶⁹ in 433
 comparison to 22 (Figure 6). Throughout the discovery of 434
 44, UCB and Proteros⁷⁰ worked together to deliver a crystal 435
 structure of a piperazine urea inhibitor bound to PI4KIIIβ that 436
 would confirm a binding mode and rationalize the observed 437
 SAR. Initial efforts to solve the structure of any protein/ligand 438
 complex were hindered by the poor behavior of PI4KIIIβ 439
 toward crystallization. Several disordered regions were 440
 identified within the protein, and it was envisaged that through 441

Table 5. Profiling of Hinge Binder Analogues of 31a

Cpd	35	38	42	44
PI4KIIIβ IC ₅₀ (nM) ^a	7	8	7	11
Hu MLR IC ₅₀ (nM) ^a	13	53	47	37
Solubility-Kinetic (μM) ^b	82	>350	>350	>350
Solubility-TD (μM) ^c	0	150	52	110
LogD (pH7.4)	2.39	1.35	1.96	1.47
hERG IC ₅₀ (μM)	8 ^d	>30	8	>30
CYP3A4 IC ₅₀ (μM)	>20 ^d	>20	>20	>20

^aIC₅₀ values are reported as means of values from at least two determinations. ^bKinetic solubility measured from DMSO stock at pH 7.4. ^cThermodynamic solubility (TD) measured from solid stock at pH 7.4. ^dFigures should be treated with caution due to low solubility.

Table 6. Comparison of ADMET Properties of 22 and Analogues with Improved Solubility

	compound			
	22	31c	38	44
Hu MLR IC ₅₀ (nM) ^a	53	31	53	37
solubility TD (μM) ^b	0	30	150	110
LogD (at pH 7.4)	1.85	2.32	1.35	1.47
MLM CL _{int} (μL·min ⁻¹ ·mg ⁻¹)	15	35	10	6
HLM CL _{int} (μL·min ⁻¹ ·mg ⁻¹)	21	14	9	4
Caco-2 ER ^c	5	1	5	2.6
Fu (mouse blood)	0.061	0.020	0.200	0.090
CL/F (mL·min ⁻¹ ·kg ⁻¹) (SD) ^d	80 (±5)	42 (±12)	46 (±3)	5.3 (±0.7)
AUC _{inf} free (h·nM) (SD) ^d	332 (±18)	205 (±56)	1746 (±112)	6941 (±887)
C _{max} free (nM) (SD) ^d	154 (±24)	194 (±27)	1087 (±186)	2113 (±259)
CL (mL·min ⁻¹ ·kg ⁻¹) ^e	— ^f	29 (±4.4)	19 (±4.0)	5 (±0.4)
AUC free (h·nM) (SD) ^e	— ^f	30 (±5)	447 (±86)	684 (±51)
t _{1/2} (h) ^e	— ^f	0.9 (±0.2)	0.8 (±0.18)	1.4 (±0.12)
V _{ss} (L·kg ⁻¹) (SD) ^e	— ^f	1.0 (±0.2)	0.8 (±0.1)	0.6 (±0.04)
oral F% ^g	— ^f	68	39	~100

^aIC₅₀ values are reported as means of values from at least two determinations. ^cCalculated from $P_{app} (A - B)/(B - A)$ in Caco-2 assay. ^dOral PK established in male Balb/C mice, $n = 3$, dosed at 10 mpk in vehicle (0.1% (w/v) Tween 80, 0.1% (w/v) silicone antifoam in 1% (w/v) methylcellulose (400 cps) in water) as homogeneous suspensions of crystalline 31c, 38, or 44. ^eI.v. PK established in male Balb/C mice, $n = 3$, dosed at 1 mpk in vehicle (30% DMA for 31c and 38 or 15% NMP for 44). ^fToo insoluble to formulate for i.v. evaluation. ^gBioavailability extrapolated from i.v./p.o. experiments.

442 reengineering of these flexible loops (a process also utilized to
 443 deliver recently published PI4KIIIβ/ligand complex struc-
 444 tures^{32,42}), constructs more amenable to crystallography could
 445 be obtained. It therefore proved possible to obtain the first
 446 crystals of a urea (44) bound to human PI4KIIIβ. These
 447 crystals consisted of two monomers of PI4KIIIβ in the
 448 asymmetric unit, with one monomer (Chain A) being well
 449 defined, while the second monomer (Chain B) was highly
 450 disordered.⁷¹ Clear density corresponding to the structure of
 451 44 was visible in the kinase domain of the ordered monomer
 452 (Chain A) and was used for all subsequent analysis of the
 453 binding mode. As expected, the amino pyrimidine of 44 makes

a bidentate interaction with the Val613 backbone, consistent
 with other published structures of amino heterocyclic
 inhibitors bound to PI4KIIIβ.^{42,44} Whereas the aryl and
 amide side chains of inhibitors such as 12 reach along the ATP
 binding pocket toward Lys564 in one direction, and Asn615 in
 the other, 44 appears to orient the appended piperazine urea
 away from the pocket toward solvent (Figure 7). There is no
 contact with Lys564, Asn615, or Tyr385, residues believed to
 be critical for PI4KIIIβ activity,⁴² although it could be
 postulated that earlier urea analogues bearing an aryl or 3-
 pyridyl group on the hinge/binding core could reach toward

X fold selectivity for PI4KIII β of **22** and **44** against members of the lipid kinase family

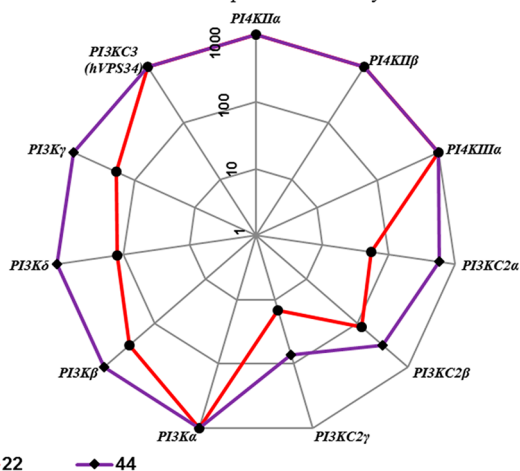


Figure 6. Radial plot showing the X-fold selectivity of **22** and **44** for PI4KIII β over 11 other lipid kinase family members.

465 Lys564 explaining the difference in potency between **14** and **22**
466 (Table 1).

467 As can be seen in Figure 7, the urea NH and carbonyl of **44**
468 form H-bonds with the main-chain Gly675 carbonyl and the
469 side-chain NH₂ of Asn390 respectively. A water molecule is
470 also visible within hydrogen-bonding range of the side-chain
471 OH of Ser618 and the urea carbonyl. The Asn390 residue is
472 part of a loop of protein that has shifted to enclose the
473 electron-rich aromatic ring of the urea in **44**, with the side-
474 chain methylene of Asn390 and the main-chain methylene of
475 Gly675 available to make putative C–H/ π interactions from
476 above and below. These interactions made by the aryl urea of
477 **44** and the loop-shifted protein could help rationalize the
478 previously observed SAR. The conformation of the piperazine,
479 the geometry of the urea carbonyl and NH, as well as the
480 electronics of the aromatic ring all needed to be optimal to give
481 the most potent compounds. For example, the change from a
482 planar nitrogen to an sp³ carbon in amide **23** meant that it
483 could not deliver the –CONHAr group on the same vector as
484 observed with **44**, resulting in a drastic loss of activity. The
485 piperazine amides (Table 2) would also be unable to replicate
486 the binding mode of **44** and suffer similar drops in activity. The
487 modest potency observed with **24d** was the exception;
488 however, it was not possible to confirm a binding mode for
489 this compound. As discussed previously, electron-rich aniline
490 ureas such as **22** appeared more potent against PI4KIII β , while
491 electron-poor ureas such as **25b** or **25e** were significantly less
492 active. This could be rationalized by ureas bearing electron-
493 donating substituents showing an increased propensity to
494 stabilize the loop movement observed in Figure 7, through
495 strengthening of the C–H/ π interactions⁷² with the Asn390
496 side chain and Gly675 backbone methylenes. Certainly, the
497 observation that the most potent compounds bear both a
498 methoxy and a methyl group suggests the effect is additive and
499 explains the jump in potency observed from **22** to **25i**,
500 although from examining the structure of **44**, there also
501 appears to be an element of space filling with this ortho
502 substituent, suggesting further exploration in this area is
503 warranted. From the crystal structure of **44**, it was also noted
504 that the chiral methyl appended to the piperazine linker sat
505 axial and pointed into a small hydrophobic pocket within the
506 active site. There was obviously a clear difference between the

(S) and (R) enantiomers, based on the data generated with 507
compounds **31a** and **31b**, and this proved to be the case for **44** 508
as well.⁷³ From experience and from examination of analogous 509
structures in the CSD,⁷⁴ the axial conformation for the chiral 510
methyl attached to piperazine is energetically favored over the 511
equatorial (results not shown). Docking was difficult for these 512
compounds because the correct geometry for the piperazine 513
nitrogen is required, and the pocket is open on two sides. A 514
protocol using ring conformations generated using Corina,⁷⁵ 515
minimized using the OPLS3 force field⁷⁶ and docked with 516
Glide,⁷⁷ was able to reproduce the crystallographic binding 517
modes. Docking of the distomer **31b** resulted in only a slightly 518
worse docking score than **31a** but with the methyl in the 519
equatorial conformation. We assume that the high eudysmic 520
ratio between these two compounds derives from higher strain 521
energy of this conformation, combined with the fact that the 522
methyl in the distomer does not fit into the hydrophobic 523
pocket shown in the X-ray structure of **44**. This apparent 524
preference for an axial substituent fitting into this small 525
hydrophobic pocket goes some way to explain the loss of 526
activity with the more complex substituted piperazines in 527
Table 4. It remains to be seen if the binding mode of **44** has 528
any relevance to the biological profile of these specific 529
PI4KIII β inhibitors, and further evaluation of the immuno- 530
logical profile of PI4KIII β inhibitors with different binding 531
modes and selectivity profiles is ongoing and will be reported 532
in future publications. To complete the assessment of **44**, it 533
was taken into the murine model of cardiac allograft rejection, 534
at a dose of 5 mpk (p.o.). With the improved oral 535
bioavailability and reduced inter-individual variability in 536
exposure of **44**, graft survival rates were significantly improved, 537
as illustrated in Figure 8. Indeed, survival rates were unaffected 538
after withdrawal of drug treatment at d14, with 90% of grafts 539
being retained at day 50 (>36 days drug free) compared with a 540
50% survival rate for **22**. With **44** confirmed as a potent 541
immunosuppressive agent, capable of prolonging heterotopic 542
allograft retention *in vivo* it positions itself as an ideal tool 543
compound to establish if PI4KIII β inhibition can play a critical 544
role in the development of future clinical immunosuppressive 545
regimens. 546

Further studies with **44** (UCB9608) and subsequent 547
analogues are being explored and will be discussed in future 548
publications. 549

CONCLUSION 550

Within this Article, we have described the discovery **44** 551
(UCB9608), an 11 nM PI4KIII β inhibitor that inhibits the 552
HuMLR response with IC₅₀ = 37 nM. Its potency and excellent 553
ADME properties make it an ideal compound for future use as 554
an *in vitro* and *in vivo* probe to elucidate the emerging role of 555
PI4KIII β inhibition in immune processes. Starting from a 556
potent yet insoluble and poorly exposed chemotype, we could 557
address both hERG and CYP3A4 inhibition liabilities by the 558
removal of a 3-pyridyl ring. Compound **22** was identified and 559
its selectivity profile against the wider kinome and the close 560
lipid kinase family established. Compound **22** was progressed 561
to murine models of T-cell-mediated antibody response, 562
showing a dose-dependent inhibition of IFN γ release in a 563
short-term mouse anti-CD3 model and significant inhibition of 564
the oxazolone-induced IgG1 response. At a dose of 100 mg/kg 565
(p.o.), **22** facilitated the survival of a heterotopic murine 566
cardiac allograft from a C57BL/6 donor mouse to a Balb/C H- 567
2 recipient. Optimization and SAR exploration led to 568

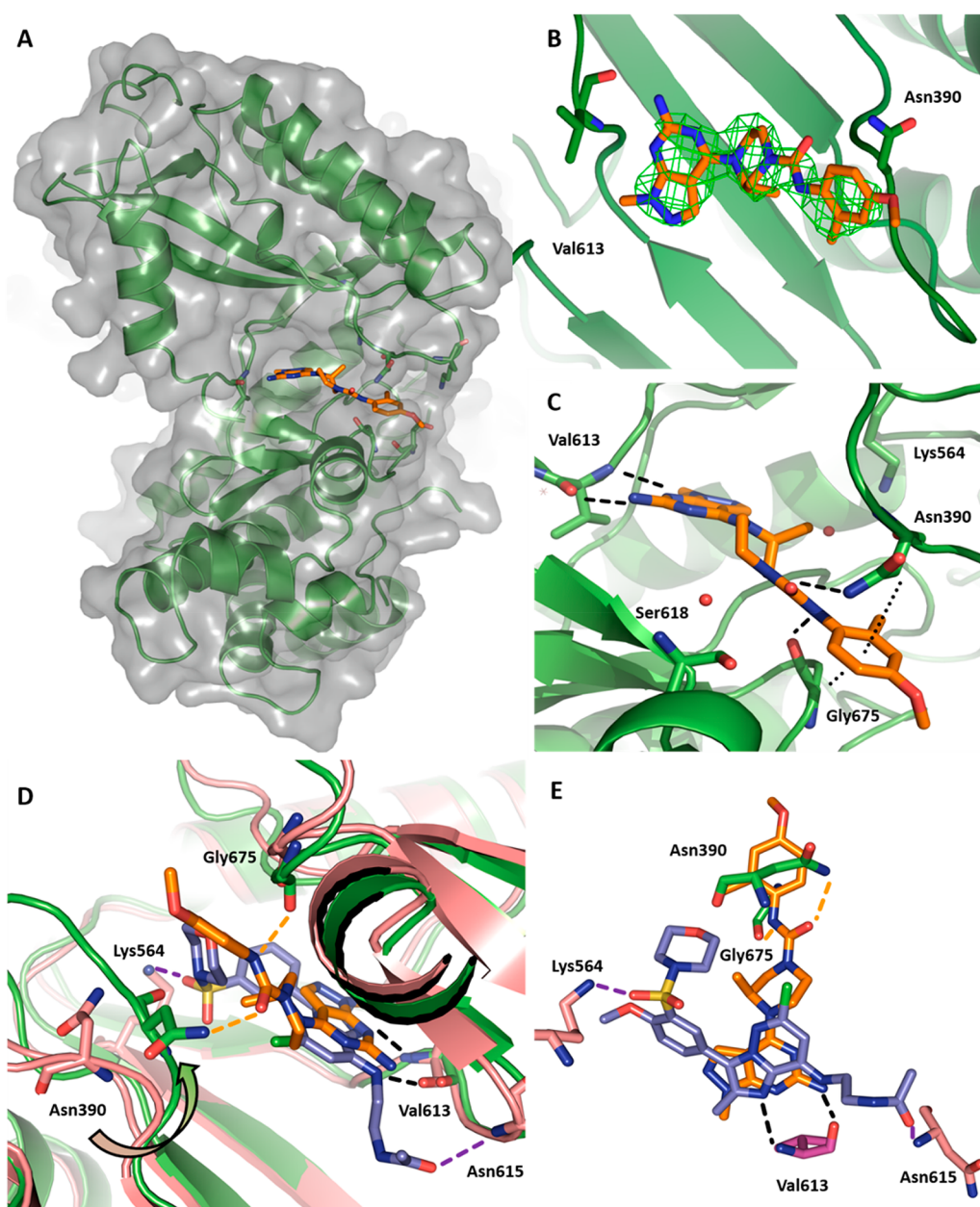


Figure 7. (A) Co-crystal of **44** (orange) and PI4KIII β (green) with surface superimposed in gray (PDB ID 6GL3). (B) The unbiased electron density ($f_o - f_c$ contoured at 3σ) of **44**. (C) Detailed view of the key protein/ligand interactions made by **44** (orange) with PI4KIII β (green). H-bonds shown as dashed lines, C–H/ π interactions as dotted lines. (D) Overlay of **44** (orange) and **12** (purple) from published structure (PDB ID 5FBL). H-bond interactions shown as dashed lines (black for shared, orange for **44**-specific, and purple for **12**-specific). Curved arrow denotes loop movement seen in structure of **44**. (E) Detailed overlay of **12** and **44**, showing key residues involved in H-bonding and the different direction of growth from the hinge-binding heterocyclic core of each ligand. Images generated using PyMol (The PyMOL Molecular Graphics System, Schrödinger, LLC).

569 compound **44** (UCB9608), which could achieve high and
 570 consistently reproducible exposures in Balb/C mice. The
 571 structure of **44** bound to PI4KIII β was solved by co-
 572 crystallization, confirming that although **44** binds to the
 573 hinge region in an analogous fashion to other published
 574 PI4KIII β inhibitors (such as **12**), it relies on a different H-
 575 bond network and unique CH/ π interaction with a shifted
 576 protein loop to deliver low nM activity. Kinase cross screening
 577 confirmed **44** to be suitably selective for PI4KIII β over other
 578 kinases, although the impact of low-level activity against the
 579 PI3KC2 family was yet to be determined. Finally, compound
 580 **44** could prevent the rejection of a heterotopic murine cardiac

581 allograft at a dose of 5 mpk. It is therefore our conclusion that
 582 **44** is an excellent example of a novel series of PI4KIII β
 583 inhibitors that rely on a unique set of interactions within the
 584 binding site to drive potency. The excellent ADME properties
 585 of **44** make it an ideal molecule to develop the understanding
 586 of the role of this novel class of PI4KIII β inhibitors on immune
 587 cell activation. Compound **44** (UCB9608) also offers an
 588 excellent platform to further develop the series as part of a
 589 potential CNI sparing treatment for the prevention of
 590 premature graft loss in solid organ transplantation, and details
 591 of these efforts will be discussed in future publications.

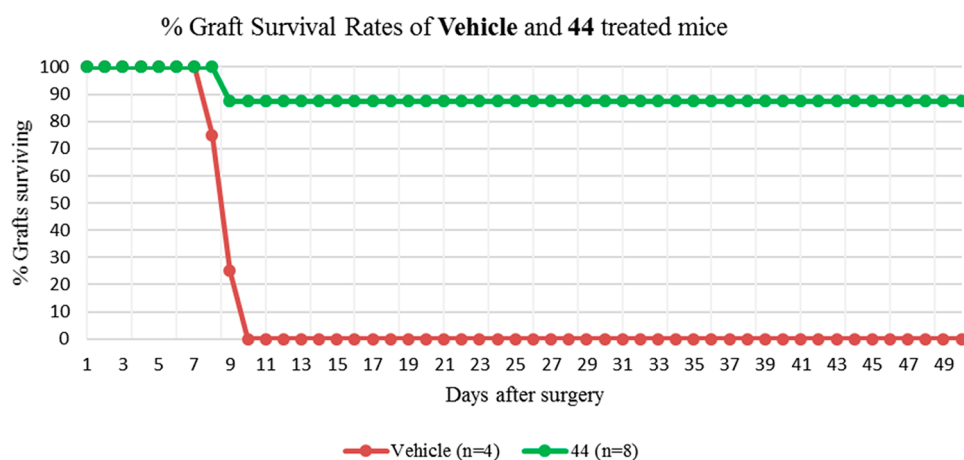


Figure 8. Comparison of survival rates for engrafted mice treated with vehicle (0.1% (w/v) Tween 80, 0.1% (w/v) silicone antifoam in 1% (w/v) methylcellulose (400 cps) in water), or **44** (5mpk in vehicle as a homogeneous suspension). Animals were dosed via oral gavage once a day for 14 days, or until a transplanted graft had ceased beating, indicative of rejection. Graft survival is defined as a strongly beating heart (as confirmed by visual inspection and palpitation).

592 ■ EXPERIMENTAL SECTION

593 Reagents and solvents were purchased from commercial sources and
 594 used without purification. All final products were >95% pure as
 595 determined by HPLC-MS on an Agilent 1100 instrument fitted with a
 596 Waters XBridge 20 × 2.1 mm, 2.5 μm column. Mobile phase was (A)
 597 10 mM ammonium formate in water + 0.1% ammonia and (B)
 598 acetonitrile + 5% mobile phase A + 0.1% ammonia. A 5 min gradient
 599 run (method 1: 5% B to 95% B in 3 min; hold until 4.00 min; at 4.01
 600 min B concentration is 5%; hold until 5 min) or a 3 min run (method
 601 2: 5% B to 95% B in 1.5 min; hold until 2.5 min; at 2.51 min B
 602 concentration is 5%; hold until 3 min) was utilized. ¹H NMR spectra
 603 were recorded at 300, 400, or 600 MHz and ¹³C NMR at 151 MHz
 604 on a Bruker spectrometer. Chemical shifts (ppm) were determined
 605 relative to internal solvent (¹H, δ 2.50 ppm; DMSO-*d*₆). Accurate
 606 Mass was determined by analysis of the samples on a calibrated
 607 Waters UPLC Xevo QToF. All animal experiments were conducted in
 608 accordance with the UK Home Office Animals (Scientific
 609 Procedures) Act 1986, with local ethical approval (in line with
 610 recently published guidelines) or with the approval of the Institutional
 611 Animal Care and Research Advisory Committee of the KU Leuven,
 612 Belgium.

613 Synthesis of **13**, **22**, **25a–k**, **31a–d**, **35**, **38**, **42**, and **44**.

614 General method 1 (isocyanate–piperazine coupling reaction): To a
 615 solution of appropriate amine (0.74 mmol) in DMF (2 mL) or DCM
 616 (2 mL) were added Et₃N (2.20 mmol) or DIPEA (2.20 mmol) and
 617 the appropriate isocyanate (0.74 mmol). The reaction mixture was
 618 stirred at room temperature for 4 h. Upon completion, the reaction
 619 mixture was concentrated, and the resulting material was purified by
 620 column chromatography (silica gel: 100–200 mesh, MeOH:DCM
 621 1:9) to afford the desired urea in yields between 20 and 95%. General
 622 method 2 (CDI coupling): To a stirred solution of the appropriate
 623 amine (0.48 mmol) in DMF (1 mL) were added DIPEA (0.44 mmol)
 624 and CDI (0.48 mmol). The reaction mixture was stirred at room
 625 temperature for 30 min. To this mixture was added a solution of **19b**
 626 (0.40 mmol) and DIPEA (0.48 mmol) in DMF (1 mL). The reaction
 627 mixture was stirred at room temperature for a further 12 h. The
 628 reaction mixture was then diluted with EtOAc, and the organic layer
 629 was washed with water and brine. The organic layer was dried over
 630 anhydrous Na₂SO₄ and concentrated *in vacuo*, and the residue was
 631 purified by column chromatography (silica: 100–200 mesh,
 632 MeOH:DCM 5–7%) to afford the desired urea in yields between
 633 20 and 95%. General method 3 (phenyl chloroformate coupling): To
 634 a solution of the appropriate amine (1.05 mmol) in THF (5 mL) at 0
 635 °C was added pyridine (0.11 mL, 1.32 mmol), followed by phenyl
 636 chloroformate (0.14 mL, 1.11 mmol). The reaction was stirred at 0
 637 °C for 2 h, and then diluted with EtOAc and washed successively with

2 M HCl solution. The organic layer was concentrated *in vacuo*, the
 resultant crude phenyl carbamate and **19b** (1 equiv) were taken up in
 DMSO (2 mL), and DIPEA (3 equiv) was added. The mixture was
 warmed to 60 °C and stirred for 3 h. After this time the reaction was
 cooled, diluted with EtOAc, and washed with water. The organic layer
 was dried over Na₂SO₄ and concentrated *in vacuo*, and the residue was
 purified by column chromatography (silica: 100–200 mesh,
 MeOH:DCM 5–7%) to afford the desired urea in yields between
 50 and 90%.

4-[5-Amino-2-(3-pyridyl)thiazolo[5,4-*d*]pyrimidin-7-yl]-*N*-(*p*-
 tolyl)piperazine-1-carboxamide (**13**) was synthesized from **21b** and 4-
 methylphenyl isocyanate according to general method 1. ¹H NMR
 (600 MHz, DMSO-*d*₆) δ 9.13 (dd, *J* = 0.9, 2.4 Hz, 1H), 8.67 (dd, *J* =
 1.6, 4.8 Hz, 1H), 8.49 (s, 1H), 8.29 (ddd, *J* = 1.6, 2.4, 8.0 Hz, 1H),
 7.56 (ddd, *J* = 0.9, 4.9, 8.1 Hz, 1H), 7.40–7.34 (m, 2H), 7.09–7.03
 (m, 2H), 6.57 (s, 2H), 4.31 (s, 4H), 3.66–3.60 (m, 4H), 2.24 (s, 3H).
¹³C NMR (151 MHz, DMSO) δ 168.58, 160.62, 155.51, 155.09,
 151.19, 150.35, 147.34, 138.29, 133.98, 131.06, 129.62, 129.21,
 125.35, 124.68, 120.25, 45.50, 44.14, 20.83. HRMS: calcd for
 C₂₂H₂₂N₈O₅ [M + H]⁺, 447.1716; found, 447.1697.

4-(5-Aminothiazolo[5,4-*d*]pyrimidin-7-yl)-*N*-(4-methoxyphenyl)-
 piperazine-1-carboxamide (**22**) was synthesized from **19b** and 4-
 methoxyphenyl isocyanate according to general method 1. ¹H NMR
 (600 MHz, DMSO-*d*₆) δ 8.71 (s, 1H), 8.43 (s, 1H), 7.39–7.33 (m,
 2H), 6.89–6.81 (m, 2H), 6.39 (s, 2H), 4.24 (s, 4H), 3.71 (s, 3H),
 3.59–3.54 (m, 4H). ¹³C NMR (151 MHz, DMSO) δ 167.59, 160.62,
 155.74, 155.38, 155.01, 143.30, 133.78, 124.68, 122.15, 114.01, 55.58,
 45.38, 44.07. HRMS: calcd for C₁₇H₁₉N₇O₂S [M + H]⁺, 386.1399;
 found, 386.1395.

4-(5-Aminothiazolo[5,4-*d*]pyrimidin-7-yl)-*N*-phenyl-piperazine-1-
 carboxamide (**25a**) was synthesized from **19b** and phenyl isocyanate
 according to general method 1. ¹H NMR (600 MHz, DMSO-*d*₆) δ
 8.72 (s, 1H), 8.58 (s, 1H), 7.50–7.45 (m, 2H), 7.28–7.22 (m, 2H),
 6.97–6.94 (m, 1H), 6.40 (s, 2H), 4.25 (s, 4H), 3.62–3.57 (m, 4H).
¹³C NMR (151 MHz, DMSO) δ 167.59, 160.62, 155.47, 155.38,
 143.31, 140.87, 128.79, 124.68, 122.28, 120.15, 45.64, 44.16. HRMS:
 calcd for C₁₆H₁₇N₇O₂S [M + H]⁺, 356.1294; found, 356.1303.

4-(5-Aminothiazolo[5,4-*d*]pyrimidin-7-yl)-*N*-(3-pyridyl)-
 piperazine-1-carboxamide (**25b**) was synthesized from **19b** and 3-
 pyridylisocyanate according to general method 1. ¹H NMR (600
 MHz, DMSO-*d*₆) δ 8.79 (s, 1H), 8.72 (s, 1H), 8.66 (d, *J* = 2.6 Hz,
 1H), 8.17 (dd, *J* = 1.5, 4.7 Hz, 1H), 7.90 (ddd, *J* = 1.6, 2.7, 8.4 Hz,
 1H), 7.29 (dd, *J* = 4.6, 8.3 Hz, 1H), 6.41 (s, 2H), 4.26 (s, 4H), 3.64–
 3.59 (m, 4H). ¹³C NMR (151 MHz, DMSO) δ 167.61, 160.62,
 155.39, 155.28, 143.35, 143.29, 141.86, 137.57, 126.96, 124.68,
 123.70, 45.38, 44.09. HRMS: calcd for C₁₅H₁₆N₈O₂S [M + H]⁺,
 357.1246; found, 357.1243.

685 4-(5-Aminothiazolo[5,4-*d*]pyrimidin-7-yl)-*N*-(6-methoxy-3-
686 pyridyl)piperazine-1-carboxamide (**25c**) was synthesized from **19b**
687 and 6-methoxy-pyridin-3-amine according to general method 2. ¹H
688 NMR (600 MHz, DMSO-*d*₆) δ 8.71 (s, 1H), 8.58 (s, 1H), 8.20 (d, *J* =
689 2.7 Hz, 1H), 7.77 (dd, *J* = 2.7, 8.9 Hz, 1H), 6.76 (d, *J* = 8.8 Hz, 1H),
690 6.40 (s, 2H), 4.27–4.23 (m, 4H), 3.81 (s, 3H), 3.61–3.56 (m, 4H).
691 ¹³C NMR (151 MHz, DMSO) δ 167.60, 160.62, 159.56, 155.74,
692 155.38, 143.34, 138.86, 133.19, 131.54, 124.67, 110.08, 53.51, 45.40,
693 44.01. HRMS: calcd for C₁₆H₁₈N₈O₂S [M + H]⁺, 387.1352; found,
694 387.1322.
695 4-(5-Aminothiazolo[5,4-*d*]pyrimidin-7-yl)-*N*-[(4-methoxyphenyl)-
696 methyl]piperazine-1-carboxamide (**25d**) was synthesized from **19b**
697 and 4-methoxybenzyl isocyanate according to general method 1. ¹H
698 NMR (600 MHz, DMSO-*d*₆) δ 8.70 (s, 1H), 7.27–7.14 (m, 2H),
699 7.09 (t, *J* = 5.8 Hz, 1H), 6.92–6.82 (m, 2H), 6.37 (s, 2H), 4.30–4.04
700 (m, 6H), 3.72 (s, 3H), 3.52–3.42 (m, 4H). ¹³C NMR (151 MHz,
701 DMSO) δ 167.56, 160.60, 158.46, 157.87, 155.37, 143.27, 133.30,
702 132.06, 128.84, 113.98, 55.50, 45.50, 43.88, 43.40. HRMS: calcd for
703 C₁₈H₂₁N₇O₂S [M + H]⁺, 400.1556; found, 400.1537.
704 4-(5-Aminothiazolo[5,4-*d*]pyrimidin-7-yl)-*N*-[4-
705 (trifluoromethoxy)phenyl]piperazine-1-carboxamide (**25e**) was syn-
706 thesized from **19b** and 4-trifluoromethoxyphenyl isocyanate according
707 to general method 1. ¹H NMR (600 MHz, DMSO-*d*₆) δ 8.79 (s, 1H),
708 8.71 (s, 1H), 7.62–7.56 (m, 2H), 7.29–7.23 (m, 2H), 6.40 (s, 2H),
709 4.25 (s, 4H), 3.62–3.57 (m, 4H). ¹³C NMR (151 MHz, DMSO) δ
710 167.60, 160.62, 155.38, 155.29, 143.34, 143.07, 140.24, 124.67,
711 121.70, 121.11, 99.99, 45.38, 44.12. HRMS: calcd for C₁₇H₁₆F₃N₇O₂S
712 [M + H]⁺, 440.1117; found, 440.1108.
713 4-(5-Aminothiazolo[5,4-*d*]pyrimidin-7-yl)-*N*-(*o*-tolyl)piperazine-1-
714 carboxamide (**25f**) was synthesized from **19b** and 2-methylphenyl
715 isocyanate according to general method 1. ¹H NMR (600 MHz,
716 DMSO-*d*₆) δ 8.71 (s, 1H), 8.11 (s, 1H), 7.24–7.17 (m, 2H), 7.14 (td,
717 *J* = 1.6, 7.7 Hz, 1H), 7.06 (td, *J* = 1.4, 7.4 Hz, 1H), 6.40 (s, 2H), 4.25
718 (s, 4H), 3.61–3.55 (m, 4H), 2.19 (s, 3H). ¹³C NMR (151 MHz,
719 DMSO) δ 167.59, 160.63, 156.05, 155.42, 143.31, 138.28, 133.60,
720 130.53, 126.48, 126.25, 125.13, 124.69, 45.32, 44.24, 18.42. HRMS:
721 calcd for C₁₇H₁₉N₇O₂S [M + H]⁺, 370.1450; found, 370.1442.
722 4-(5-Aminothiazolo[5,4-*d*]pyrimidin-7-yl)-*N*-(*m*-tolyl)piperazine-
723 1-carboxamide (**25g**) was synthesized from **19b** and 3-methylphenyl
724 isocyanate according to general method 1. ¹H NMR (600 MHz,
725 DMSO-*d*₆) δ 8.71 (s, 1H), 8.51 (s, 1H), 7.31 (s, 1H), 7.28 (d, *J* = 8.1
726 Hz, 1H), 7.13 (t, *J* = 7.8 Hz, 1H), 6.77 (d, 7.5 Hz, 1H), 6.40 (s, 2H),
727 4.24 (s, 4H), 3.61–3.55 (m, 4H), 2.26 (s, 3H). ¹³C NMR (151 MHz,
728 DMSO) δ 167.59, 160.62, 155.46, 155.38, 143.31, 140.77, 137.81,
729 128.64, 124.67, 123.01, 120.74, 117.30, 45.47, 44.15, 21.67. HRMS:
730 calcd for C₁₇H₁₉N₇O₂S [M + H]⁺, 370.1450; found, 370.1446.
731 4-(5-Aminothiazolo[5,4-*d*]pyrimidin-7-yl)-*N*-(*p*-tolyl)piperazine-1-
732 carboxamide (**25h**) was synthesized from **19b** and 4-methylphenyl
733 isocyanate according to general method 1. ¹H NMR (600 MHz,
734 DMSO-*d*₆) δ 8.71 (s, 1H), 8.48 (s, 1H), 7.38–7.32 (m, 2H), 7.08–
735 7.03 (m, 2H), 6.40 (s, 2H), 4.24 (s, 4H), 3.60–3.55 (m, 4H), 2.24 (s,
736 3H). ¹³C NMR (151 MHz, DMSO) δ 167.59, 160.62, 155.55, 155.38,
737 143.30, 138.25, 131.09, 129.21, 124.68, 120.36, 45.42, 44.10, 20.82.
738 HRMS: calcd for C₁₇H₁₉N₇O₂S [M + H]⁺, 370.1450; found, 370.1436.
739 4-(5-Aminothiazolo[5,4-*d*]pyrimidin-7-yl)-*N*-(4-methoxy-2-
740 methylphenyl)piperazine-1-carboxamide (**25i**) was synthesized from
741 **19b** and 4-methoxy-2-methylphenyl isocyanate according to general
742 method 1. ¹H NMR (600 MHz, DMSO-*d*₆) δ 8.71 (s, 1H), 8.01 (s,
743 1H), 7.06 (d, *J* = 8.6 Hz, 1H), 6.78 (d, *J* = 2.9 Hz, 1H), 6.71 (dd, *J* =
744 3.0, 8.6 Hz, 1H), 6.40 (s, 2H), 4.24 (s, 4H), 3.73 (s, 3H), 3.58–3.53
745 (m, 4H), 2.15 (s, 3H). ¹³C NMR (151 MHz, DMSO) δ 167.59,
746 160.63, 157.08, 156.46, 155.41, 143.30, 135.87, 131.05, 128.42,
747 124.67, 115.62, 111.45, 55.55, 45.06, 44.20, 18.61. HRMS: calcd for
748 C₁₈H₂₁N₇O₂S [M + H]⁺, 400.1561; found, 400.1549.
749 4-(5-Aminothiazolo[5,4-*d*]pyrimidin-7-yl)-*N*-(6-methoxy-4-meth-
750 yl-3-pyridyl)piperazine-1-carboxamide (**25j**) was synthesized from
751 **19b** and 6-methoxy-4-methyl-pyridin-3-amine according to general
752 method 3. ¹H NMR (600 MHz, DMSO-*d*₆) δ 8.71 (s, 1H), 8.19 (s,
753 1H), 7.89 (s, 1H), 6.70 (s, 1H), 6.40 (s, 2H), 4.25 (s, 4H), 3.81 (s,
754 3H), 3.60–3.55 (m, 4H), 2.15 (s, 3H). ¹³C NMR (151 MHz,

DMSO) δ 167.60, 161.74, 160.63, 156.46, 155.42, 147.87, 144.71, 755
143.33, 129.67, 124.68, 110.93, 53.52, 45.35, 44.20, 18.00. HRMS: 756
calcd for C₁₇H₂₀N₈O₂S [M + H]⁺, 401.1508; found, 401.1505. 757

4-(5-Aminothiazolo[5,4-*d*]pyrimidin-7-yl)-*N*-(6-methoxy-2-meth- 758
yl-3-pyridyl)piperazine-1-carboxamide (**25k**) was synthesized from 759
19b and 6-methoxy-2-methyl-pyridin-3-amine according to general 760
method 3. ¹H NMR (600 MHz, DMSO-*d*₆) δ 8.71 (s, 1H), 8.16 (s, 761
1H), 7.46 (d, *J* = 8.6 Hz, 1H), 6.61 (d, *J* = 8.5 Hz, 1H), 6.40 (s, 2H), 762
4.25 (s, 4H), 3.82 (s, 3H), 3.60–3.55 (m, 4H), 2.29 (s, 3H). ¹³C 763
NMR (151 MHz, DMSO) δ 167.60, 160.62, 160.55, 156.25, 155.41, 764
151.90, 143.33, 138.72, 127.77, 124.68, 107.69, 53.48, 45.28, 44.15, 765
21.21. HRMS: calcd for C₁₇H₂₀N₈O₂S [M + H]⁺, 401.1508; found, 766
401.1506. 767

(3S)-4-(5-Aminothiazolo[5,4-*d*]pyrimidin-7-yl)-*N*-(4-methoxy-2- 768
methyl-phenyl)-3-methyl-piperazine-1-carboxamide (**31a**) was syn- 769
thesized from **30a** and 4-methoxy-2-methylphenyl isocyanate 770
according to general method 1. ¹H NMR (600 MHz, DMSO-*d*₆) δ 771
8.71 (s, 1H), 7.98 (s, 1H), 7.04 (d, *J* = 8.6 Hz, 1H), 6.78 (d, *J* = 2.9 772
Hz, 1H), 6.71 (dd, *J* = 3.0, 8.6 Hz, 1H), 6.37 (s, 2H), 5.60 (s, 1H), 773
5.15 (s, 1H), 4.15–4.11 (m, 1H), 4.01–3.96 (m, 1H), 3.73 (s, 3H), 774
3.38 (s, 1H), 3.26 (dd, *J* = 3.9, 13.4 Hz, 1H), 3.08–3.02 (m, 1H), 775
2.15 (s, 3H), 1.26 (d, *J* = 6.6 Hz, 3H). ¹³C NMR (151 MHz, DMSO) 776
δ 167.63, 160.64, 157.13, 156.57, 155.28, 143.14, 136.05, 131.09, 777
128.58, 124.59, 115.61, 111.47, 55.55, 47.91, 44.00, 40.53, 40.39, 778
18.55, 15.57. HRMS: calcd for C₁₉H₂₃N₇O₂S [M + H]⁺, 414.1712; 779
found, 414.1708. 780

(3R)-4-(5-Aminothiazolo[5,4-*d*]pyrimidin-7-yl)-*N*-(4-methoxy-2- 781
methyl-phenyl)-3-methyl-piperazine-1-carboxamide (**31b**) was syn- 782
thesized from **30b** and 4-methoxy-2-methylphenyl isocyanate 783
according to general method 1. ¹H NMR (600 MHz, DMSO-*d*₆) δ 784
8.71 (s, 1H), 7.98 (s, 1H), 7.04 (d, *J* = 8.6 Hz, 1H), 6.78 (d, *J* = 2.9 785
Hz, 1H), 6.71 (dd, *J* = 3.0, 8.6 Hz, 1H), 6.37 (s, 2H), 5.60 (s, 1H), 786
5.15 (s, 1H), 4.15–4.11 (m, 1H), 4.01–3.96 (m, 1H), 3.73 (s, 3H), 787
3.38 (s, 1H), 3.26 (dd, *J* = 3.9, 13.4 Hz, 1H), 3.08–3.02 (m, 1H), 788
2.15 (s, 3H), 1.26 (d, *J* = 6.6 Hz, 3H). ¹³C NMR (151 MHz, DMSO) 789
δ 167.63, 160.64, 157.13, 156.57, 155.28, 143.14, 136.05, 131.09, 790
128.58, 124.59, 115.61, 111.47, 55.55, 47.91, 44.00, 40.53, 40.39, 791
18.55, 15.57. HRMS: calcd for C₁₉H₂₃N₇O₂S [M + H]⁺, 414.1712; 792
found, 414.1708. 793

(3S)-4-(5-Aminothiazolo[5,4-*d*]pyrimidin-7-yl)-*N*-(4-methoxy- 794
phenyl)-3-methyl-piperazine-1-carboxamide (**31c**) was synthesized 795
from **30a** and 4-methoxyphenyl isocyanate according to general 796
method 1. ¹H NMR (600 MHz, DMSO-*d*₆) δ 8.71 (s, 1H), 8.38 (s, 797
1H), 7.38–7.33 (m, 2H), 6.87–6.82 (m, 2H), 6.37 (s, 2H), 5.58 (s, 798
1H), 5.15 (s, 1H), 4.15–4.09 (m, 1H), 4.02–3.96 (m, 1H), 3.71 (s, 799
3H), 3.45–3.34 (m, 1H), 3.25 (dd, *J* = 4.0, 13.4 Hz, 1H), 3.09–3.03 800
(m, 1H), 1.23 (d, *J* = 6.6 Hz, 3H). ¹³C NMR (151 MHz, DMSO) δ 801
167.62, 160.63, 156.08, 155.23, 155.03, 143.15, 133.77, 124.59, 802
122.27, 113.99, 55.59, 47.78, 44.12, 40.38, 40.24, 15.80. HRMS: calcd 803
for C₁₈H₂₁N₇O₂S [M + H]⁺, 400.1556; found, 400.1541. 804

(3S)-4-(5-Aminothiazolo[5,4-*d*]pyrimidin-7-yl)-*N*-(6-methoxy-2- 805
methyl-3-pyridyl)-3-methyl-piperazine-1-carboxamide (**31d**) was syn- 806
thesized from **30a** and 6-methoxy-2-methyl-pyridin-3-amine accord- 807
ing to general method 3. ¹H NMR (600 MHz, DMSO-*d*₆) δ 8.71 (s, 808
1H), 8.12 (s, 1H), 7.44 (d, *J* = 8.5 Hz, 1H), 6.61 (d, *J* = 8.5 Hz, 1H), 809
6.37 (s, 2H), 5.60 (s, 1H), 5.16 (s, 1H), 4.17–4.09 (m, 1H), 4.01– 810
3.96 (m, 1H), 3.82 (s, 3H), 3.43–3.38 (m, 1H), 3.29 (dd, *J* = 4.0, 811
13.5 Hz, 1H), 3.11–3.04 (m, 1H), 2.29 (s, 3H), 1.26 (d, *J* = 6.6 Hz, 812
3H). ¹³C NMR (151 MHz, DMSO) δ 167.64, 160.63, 160.60, 156.36, 813
155.27, 152.07, 143.18, 138.86, 127.80, 124.61, 107.72, 53.49, 47.89, 814
43.98, 40.53, 40.38, 21.13, 15.71. HRMS: calcd for C₁₈H₂₂N₈O₂S [M 815
+ H]⁺, 415.1665; found, 415.1645. 816

(3S)-4-(2-aminothieno[2,3-*d*]pyrimidin-4-yl)-*N*-(4-methoxy-2- 817
methyl-phenyl)-3-methyl-piperazine-1-carboxamide (**35**) was synthe- 818
sized from **34** and 4-methoxy-2-methylphenyl isocyanate according to 819
general method 1. ¹H NMR (600 MHz, DMSO-*d*₆) δ 7.97 (s, 1H), 820
7.33 (d, *J* = 6.2 Hz, 1H), 7.06–7.00 (m, 2H), 6.78 (d, *J* = 2.9 Hz, 821
1H), 6.71 (dd, *J* = 3.1, 8.6 Hz, 1H), 6.19 (s, 2H), 4.80–4.74 (m, 1H), 822
4.35–4.29 (m, 1H), 4.09–4.00 (m, 1H), 3.96–3.88 (m, 1H), 3.73 (s, 823
3H), 3.47–3.40 (m, 1H), 3.33–3.27 (m, 1H), 3.17–3.09 (m, 1H), 824

825 2.14 (s, 3H), 1.28 (d, $J = 6.7$ Hz, 3H). ^{13}C NMR (151 MHz, DMSO)
826 δ 172.32, 160.22, 158.84, 157.09, 156.61, 136.00, 131.12, 128.51,
827 122.00, 115.61, 115.28, 111.46, 108.80, 55.56, 49.82, 47.76, 43.62,
828 40.68, 18.55, 15.75. HRMS: calcd for $\text{C}_{20}\text{H}_{24}\text{N}_6\text{O}_2\text{S}$ [$\text{M} + \text{H}$] $^+$,
829 413.1760; found, 413.1756.

830 (3*S*)-4-(2-amino-9-methyl-purin-6-yl)-*N*-(4-methoxy-2-methyl-
831 phenyl)-3-methyl-piperazine-1-carboxamide (**38**) was synthesized
832 from **37** and 4-methoxy-2-methylphenyl isocyanate according to
833 general method 1. ^1H NMR (600 MHz, DMSO- d_6) δ 7.97 (s, 1H),
834 7.73 (s, 1H), 7.03 (d, $J = 8.6$ Hz, 1H), 6.78 (d, $J = 2.9$ Hz, 1H), 6.71
835 (dd, $J = 3.0, 8.6$ Hz, 1H), 5.91 (s, 2H), 5.55 (s, 1H), 5.04 (s, 1H),
836 4.17–4.12 (m, 1H), 4.02–3.98 (m, 1H), 3.73 (s, 3H), 3.56 (s, 3H),
837 3.31–3.22 (m, 1H), 3.19 (dd, $J = 3.8, 13.4$ Hz, 1H), 3.00–2.92 (m,
838 1H), 2.15 (s, 3H), 1.22 (d, $J = 6.7$ Hz, 3H). ^{13}C NMR (151 MHz,
839 DMSO) δ 160.07, 157.11, 156.58, 153.95, 153.93, 137.83, 136.07,
840 131.15, 128.60, 115.61, 113.75, 111.46, 55.55, 48.03, 44.06, 40.53,
841 40.39, 29.51, 18.56, 15.40. HRMS: calcd for $\text{C}_{20}\text{H}_{26}\text{N}_8\text{O}_2$ [$\text{M} + \text{H}$] $^+$,
842 411.2257; found, 411.2258.

843 2-Amino-4-[4-(4-methoxy-2-methylphenylcarbamoyl)-2-(*S*)-meth-
844 ylpiperazin-1-yl]-isothiazolo[5,4-*d*]pyrimidine (**42**) was synthesized
845 from **41** and 4-methoxy-2-methylphenyl isocyanate according to
846 general method 1. ^1H NMR (600 MHz, DMSO- d_6) δ 8.91 (s, 1H),
847 8.00 (s, 1H), 7.04 (d, $J = 8.6$ Hz, 1H), 6.78 (d, $J = 2.9$ Hz, 1H), 6.74
848 (s, 2H), 6.73–6.69 (m, 1H), 4.90–4.81 (m, 1H), 4.49–4.40 (m, 1H),
849 4.09–4.02 (m, 1H), 3.98–3.93 (m, 1H), 3.73 (s, 3H), 3.60–3.51 (m,
850 1H), 3.41–3.31 (m, 1H), 3.25–3.18 (m, 1H), 2.14 (s, 3H), 1.31 (d, J
851 = 6.6 Hz, 3H). ^{13}C NMR (151 MHz, DMSO) δ 184.06, 161.38,
852 158.76, 157.12, 156.59, 154.25, 136.00, 131.07, 128.50, 115.62,
853 111.48, 108.12, 55.56, 47.49, 43.48, 40.53, 40.39, 18.55, 16.25.
854 HRMS: calcd for $\text{C}_{19}\text{H}_{23}\text{N}_7\text{O}_2\text{S}$ [$\text{M} + \text{H}$] $^+$, 414.1712; found,
855 414.1706.

856 (3*S*)-4-(6-Amino-1-methyl-pyrazolo[3,4-*d*]pyrimidin-4-yl)-*N*-(4-
857 methoxy-2-methyl-phenyl)-3-methyl-piperazine-1-carboxamide (**44**)
858 was synthesized from **43** and 4-methoxy-2-methylphenyl isocyanate
859 according to general method 1. ^1H NMR (600 MHz, DMSO- d_6) δ
860 8.00 (s, 1H), 7.93 (s, 1H), 7.04 (d, $J = 8.6$ Hz, 1H), 6.78 (d, $J = 3.0$
861 Hz, 1H), 6.71 (dd, $J = 3.0, 8.6$ Hz, 1H), 6.20 (s, 2H), 4.97–4.58 (m,
862 1H), 4.58–4.20 (m, 1H), 4.13–4.06 (m, 1H), 4.01–3.95 (m, 1H),
863 3.73 (s, 3H), 3.71 (s, 3H), 3.44–3.32 (m, 1H), 3.31–3.25 (m, 1H),
864 3.14–3.07 (m, 1H), 2.15 (s, 3H), 1.24 (d, $J = 6.7$ Hz, 3H). ^{13}C NMR
865 (101 MHz, DMSO, 100 $^\circ\text{C}$) δ 161.99, 157.67, 157.61, 157.34, 156.82,
866 135.63, 133.06, 131.46, 128.20, 115.97, 111.77, 95.53, 55.81, 48.98,
867 47.81, 43.88, 41.19, 33.40, 18.33, 15.96. HRMS: calcd for
868 $\text{C}_{20}\text{H}_{26}\text{N}_8\text{O}_2$ [$\text{M} + \text{H}$] $^+$, 411.2257; found, 411.2254.

869 **Biological Screening Assays. Mixed Lymphocyte Reaction**
870 (*MLR*) *Test*. Human peripheral blood mononuclear cells (PBMCs)
871 were isolated from buffy coats, obtained from healthy blood donors by
872 Ficoll (Lymphoprep, Axis-Shield PoC AS, Oslo, Norway) density-
873 gradient centrifugation. The cells at the Ficoll-plasma interface were
874 washed three times and used as “responder” cells. RPMI 1788
875 (ATCC, no. CCL-20 156) cells were treated with mitomycin C
876 (Kyowa, Nycomed, Brussels, Belgium) and used as “stimulator” cells.
877 Responder cells (0.12 \times 10 6), stimulator cells (0.045 \times 10 6), and
878 compounds (in different concentrations) were co-cultured for 6 days
879 in RPMI 1640 medium (BioWhittaker, Lonza, Belgium) supple-
880 mented with 10% fetal calf serum, 100 U/mL Geneticin (Gibco,
881 LifeTechnologies, UK). Cells were cultured in triplicate in flat-
882 bottomed 96-well microtiter tissue culture plates (TTP, Switzerland).
883 After 5 days, cells were pulsed with 1 μCi of methyl-3H thymidine
884 (MP Biomedicals, USA), harvested after 18 h on glass filter paper, and
885 counted. Proliferation values were expressed as counts per minute
886 (cpm) and converted to % inhibition with respect to a blank MLR test
887 (identical but without added compound). The IC_{50} was determined
888 from a graph with at least four points, each derived from the mean of
889 two experiments. The IC_{50} value represents the lowest concentration
890 of test compound (expressed in μM) that resulted in a 50% inhibition
891 of the MLR.

892 **PI4KIII β Enzyme Inhibition Assay.** Compounds were screened in
893 1% DMSO (final) as 3-fold serial dilutions from a starting
894 concentration of 20 μM . PI4KIII β , PI Lipid Kinase Substrate (both

Invitrogen, Paisley UK), ATP (Promega, Southampton, UK), and the
895 SX compounds were prepared in 20 mM Tris pH 7.5, 0.5 mM EGTA,
896 2 mM DTT, 5 mM MgCl_2 , 0.4% Triton (all Sigma, Dorset, UK). The
897 final 25 μL kinase reaction consisted of 4 nM PI4KIII β , 100 μM PI
898 Lipid Kinase Substrate (both Invitrogen), and compound. The final
899 ATP concentration in the assay was 10 μM . Briefly, compound was
900 added to PI4KIII β followed by addition of ATP/PI Lipid Kinase
901 Substrate mixture. The reaction mixture was incubated for 60 min at
902 room temperature. The ADP-Glo Reagent was added, and the plate
903 was incubated for 40 min at room temperature, followed by addition
904 of ADP-Glo Detect Reagent (both Promega, Southampton, UK). The
905 plate was incubated for a further 120 min and luminescence read on a
906 plate reader. The IC_{50} values were generated with a 4PL fit using XLfit
907 software. 908

909 **In Vitro DMPK Methods and hERG Screening.** For methods
910 pertaining to measuring microsomal clearances (human and mouse),
911 blood binding (mouse), passive permeability (Caco-2), and
912 cytochrome P450 inhibition (3A4 and other isoforms), see methods
913 described by Cyprotex (<http://www.cyprotex.com/admeqk>, accessed
914 May 23, 2018). hERG Screening was carried out by B'SYS ([http://](http://www.bsych.ch/services/ion-channel-screening/patch-clamping/herg-cho.html)
915 [www.bsych.ch/services/ion-channel-screening/patch-clamping/herg-](http://www.bsych.ch/services/ion-channel-screening/patch-clamping/herg-cho.html)
916 [cho.html](http://www.bsych.ch/services/ion-channel-screening/patch-clamping/herg-cho.html), accessed May 23, 2018).

917 **Evaluation in Murine Heart Allograft Model.** Inbred C57BL/6 H-
918 2b and Balb/C female mice, 8–10 weeks old, between 20 and 25 g
919 were used as donor and recipient, respectively. Heterotopic heart
920 transplantation was performed by implanting the donor heart on the
921 neck of the recipient using conventional microsurgery techniques as
922 described previously.⁷⁸ Grafts were implanted in the recipient neck,
923 and graft beating was checked daily by inspection and palpitation.
924 Cessation of beating indicated graft rejection, which was confirmed by
925 histological examination. Housing and all experimental animal
926 procedures were approved by the Institutional Animal Care and
927 Research Advisory Committee of the KU Leuven, Belgium. 927

928 **Structural Determination of **44** Bound to PI4KIII β .** *Protein*
929 *Production for Crystallography.* For structure analysis, a crystal-
930 lization system was developed for the kinase domain of PI4KIII β , in
931 which amino acids 429–531 of PI4KIII β were replaced by a short
932 linker sequence. In summary,⁷⁹ protein carrying an N-terminal TEV-
933 cleavable HIS-GST fusion was expressed in baculovirus-infected
934 insect cells and purified by a three-step procedure comprising affinity
935 and size exclusion chromatography steps. Protein for crystallization
936 was concentrated to 15–20 mg/mL in crystallization buffer (20 mM
937 HEPES/NaOH, pH = 7.0, 150 mM NaCl, 10% glycerol, 5 mM DTT)
938 and stored in small aliquots at 193 K. 938

939 **Crystallization and Structure Analysis.** Crystals of PI4KIII β in
940 complex with **44** were grown by mixing protein solution (12.5 mg/
941 mL + 0.5 mM TCEP + 5 mM MgCl_2 + 2 mM ligand **44**) with
942 reservoir solution (0.2 M sodium citrate, 22% (w/v) PEG3350, 10
943 mM manganese(II) chloride) in a 1:1 ratio at 293 K. Before flash
944 freezing in liquid nitrogen, crystals were cryo protected by immersing
945 them in reservoir solution supplemented with 20% (v/v) PEG200.
946 Diffraction data of the complex were collected at the Swiss Light
947 Source (SLS, Villigen, Switzerland). The structure was solved to a
948 final resolution of 2.77 Å. The phase information necessary to
949 determine and analyze the structure was obtained by molecular
950 replacement using a previously solved structure of PI4KIII β as a
951 search model.⁸⁰ Subsequent model building and refinement was
952 performed according to standard protocols with CCP4⁸¹ and
953 COOT.⁸² Ligand parametrization and generation was carried out
954 with CORINA.⁸³ The water model was built with the “find waters2”
955 algorithm of COOT, followed by refinement with REFMAC5⁸⁴ and
956 checking all waters with the validation tool of COOT. The crystals
957 contain two monomers of human PI4KIII β protein (Chain A and
958 Chain B) in the asymmetric unit, with only one of the two protein
959 monomers having ligand **44** bound (Chain A). Chain A is well-
960 defined by electron density, with an average *B*-factor after TLS
961 analysis of 56.86. In Chain B, lacking a bound ligand, the electron
962 density is much weaker, and a large portion of the N-lobe is poorly
963 defined (average *B*-factor of 95.77⁷¹), hence the higher than normal
964 *R*-factors observed (R [%]/ R_{free} [%] = 27.6/33.3), given the 964

965 resolution of the structure (2.77 Å). Full data collection, processing,
966 and refinement statistics for the structure of **44** bound to human
967 PI4KIIIβ are given in the [Supporting Information](#).

968 ■ ASSOCIATED CONTENT

969 ● Supporting Information

970 The Supporting Information is available free of charge on the
971 [ACS Publications website](#) at DOI: [10.1021/acs.jmed-](https://doi.org/10.1021/acs.jmedchem.8b00521)
972 [chem.8b00521](https://doi.org/10.1021/acs.jmedchem.8b00521).

973 Full experimental details and characterization of
974 intermediates **16**, **17**, **18**, **19a,b**, **20**, **21a,b**, **29a,b**,
975 **30a,b**, **33**, **34**, **37**, **40**, **41**, and **43**, and compounds **11**,
976 **23**, **24a–f**, and **28a–g**; further details on the structural
977 determination of PI4KIIIβ with **44** (including refine-
978 ment statistics); kinase profiling of **2**, **13**, **22**, and **44**;
979 details of physicochemical assays used; reactive metab-
980 olite screening method and results for **22** and **44** and the
981 *in vivo* methods for anti-CD3 and OXA models ([PDF](#))
982 Full list of molecular formula strings ([CSV](#))

983 Accession Codes

984 The atomic coordinates and structure factors for compound **44**
985 (UCB9608) are deposited in the RCSB Protein Data Bank,
986 www.pdb.org (accession code 6GL3), and authors will release
987 the atomic coordinates and experimental data upon article
988 publication.

989 ■ AUTHOR INFORMATION

990 Corresponding Author

991 *Phone: +44-1753-534655. E-mail: [james.reuberson@ucb.](mailto:james.reuberson@ucb.com)
992 [com](mailto:james.reuberson@ucb.com).

993 ORCID

994 James Reuberson: [0000-0001-9146-0771](https://orcid.org/0000-0001-9146-0771)

995 Piet Herdewijn: [0000-0003-3589-8503](https://orcid.org/0000-0003-3589-8503)

996 Will Pitt: [0000-0001-8164-4550](https://orcid.org/0000-0001-8164-4550)

997 Present Address

998 ^{||}B.V.: Center for Drug Design and Discovery, Bioincubator 2,
999 Gaston Geenslaan 2, 3001 Leuven, Belgium

1000 Notes

1001 The authors declare no competing financial interest.

1002 ■ ACKNOWLEDGMENTS

1003 Special thanks to Rodger Allen, Johnny Zhu, and Jeremy Davis
1004 for their support and guidance. Recognition to Anant
1005 Ghawalkar and the SAI team for their synthetic contributions,
1006 to Justin Staniforth, Richard Taylor, Harry Mackenzie, and the
1007 PASG team for analytical support, Mike King for CADD input
1008 and discussions, and Doug Byrne and Sukhjit Sohal for help
1009 with standard synthesis. Thanks also to Alex Ferecsko, Sophie
1010 Kervyn, Lloyd King, Franck Atienza, and Helga Gerets for their
1011 help in formulation, safety profiling, and establishing met ID.
1012 In memory of P.L.R.

1013 ■ ABBREVIATIONS USED

1014 ADME, absorption, distribution, metabolism, and excretion;
1015 AUC, area under the curve; Boc, *tert*-butoxycarbamate; CDI,
1016 carbonyl diimidazole; CNI, calcineurin inhibitor; Cps, cycles
1017 per second; CSA, cyclosporin A; CYP, cytochrome P; DBU,
1018 1,8-diazabicyclo[5.4.0]undec-7-ene; DCM, dichloromethane;
1019 DDI, drug–drug interaction; DIPEA, diisopropylethylamine;
1020 DMF, dimethylformamide; DMSO, dimethyl sulfoxide; EDCl,
1021 1-ethyl-3-(3-(dimethylamino)propyl)carbodiimide; ELISA, en-

zyme-linked immunosorbent assay; Et₃N, triethylamine; 1022
EtOAc, ethyl acetate; FU, fraction unbound; HATU, 1- 1023
[bis(dimethylamino)methylene]-1*H*-1,2,3-triazolo[4,5-*b*]- 1024
pyridinium 3-oxid hexafluorophosphate; HBA, hydrogen bond 1025
acceptor; HBD, hydrogen bond donor; HLM, human liver 1026
microsome; HOBt, hydroxybenzotriazole; HuMLR, human 1027
mixed lymphocyte reaction; IFN, interferon; MeOH, meth- 1028
anol; MLM, mouse liver microsomes; MMF, mycophenolate 1029
mofetil; MPF, multiplate format; mpk, milligrams per kilo- 1030
gram; NADPH, nicotinamide adenine dinucleotide phosphate; 1031
NBS, *N*-bromosuccinimide; NMP, *N*-methylpyrrolidinone; 1032
PI3KCl, phosphoinositol-3-kinase class 1; PI3KCl2, phospho- 1033
inositol-3-kinase class 2; PI4KIIIβ, phosphoinositol-4-kinase 1034
class 3 beta; PK, pharmacokinetic; *p.o.*, *per os*; PyBOP, 1035
(benzotriazol-1-yloxy)tripyrrolidinophosphonium hexafluoro- 1036
phosphate; SAR, structure–activity relationship 1037

1038 ■ REFERENCES

- 1039 (1) Dangoor, J. Y.; Hakim, D. N.; Singh, R. P.; Hakim, N. S. 1040
Transplantation: A Brief History. *Exp. Clin. Transplant.: Off. J. Middle* 1041
East Soc. Organ Transplant. **2015**, *13*, 1–5.
- 1042 (2) Agarwal, A.; Ally, W.; Brayman, K. The Future Direction and 1043
Unmet Needs of Transplant Immunosuppression. *Expert Rev. Clin.* 1044
Pharmacol. **2016**, *9*, 873–876.
- 1045 (3) Billingham, R. E.; Krohn, P. L.; Medawar, P. B. Effect of 1046
Cortisone on Survival of Skin Homografts in Rabbits. *Br. Med. J.* 1047
1951, *1*, 1157–1163.
- 1048 (4) Borel, J. F.; Kis, Z. L. The Discovery and Development of 1049
Cyclosporine (Sandimmune). *Transplant. Proc.* **1991**, *23*, 1867–1874.
- 1050 (5) Goto, T.; Kino, T.; Hatanaka, H.; Nishiyama, M.; Okuhara, M.; 1051
Kohsaka, M.; Aoki, H.; Imanaka, H. Discovery of FK-506, a Novel 1052
Immunosuppressant Isolated from *Streptomyces Tsukubaensis*. 1053
Transplant. Proc. **1987**, *19*, 4–8.
- 1054 (6) Sollinger, H. W. Mycophenolates in Transplantation. *Clin.* 1055
Transplant. **2004**, *18*, 485–492.
- 1056 (7) Salvadori, M.; Bertoni, E. Is it Time to Give Up with Calcineurin 1057
Inhibitors in Kidney Transplantation? *World J. Transplant.* **2013**, *3*, 1058
7–25.
- 1059 (8) Klintmalm, G. B.; Vincenti, F.; Kirk, A. Steroid-Responsive 1060
Acute Rejection Should Not Be the End Point for Immunosuppres- 1061
sive Trials. *Am. J. Transplant.* **2016**, *16*, 3077–3078.
- 1062 (9) Flechner, S. M.; Kobashigawa, J.; Klintmalm, G. Calcineurin 1063
Inhibitor-Sparing Regimens in Solid Organ Transplantation: Focus on 1064
Improving Renal Function and Nephrotoxicity. *Clin. Transplant.* 1065
2008, *22*, 1–15.
- 1066 (10) Jang, M. Y.; Lin, Y.; De Jonghe, S.; Gao, L. J.; Vanderhoydonck, 1067
B.; Froeyen, M.; Rozenski, J.; Herman, J.; Louat, T.; Van Belle, K.; 1068
Waer, M.; Herdewijn, P. Discovery of 7-*N*-piperazinylthiazolo[5,4- 1069
d]pyrimidine Analogues as a Novel Class of Immunosuppressive 1070
Agents with *in Vivo* Biological Activity. *J. Med. Chem.* **2011**, *54*, 655– 1071
668.
- 1072 (11) Ghobrial, II; Morris, A. G.; Booth, L. J. Clinical Significance of 1073
in Vitro Donor-Specific Hyporesponsiveness in Renal Allograft 1074
Recipients as Demonstrated by the MLR. *Transplant Int.* **1994**, *7*, 1075
420–427.
- 1076 (12) Ferraris, J.; Tambutti, M.; Prigoshin, N. Improved Long-Term 1077
Graft Function in Kidney Transplant Recipients with Donor Antigen- 1078
Specific Hyporeactivity. *Pediatr. Transplant.* **2007**, *11*, 139–144.
- 1079 (13) Thomas, F. T.; Lee, H. M.; Lower, R. R.; Thomas, J. M. 1080
Immunological Monitoring as a Guide to the Management of 1081
Transplant Recipients. *Surg. Clin. North Am.* **1979**, *59*, 253–281.
- 1082 (14) Cerep (now Eurofins): [https://www.eurofinsdiscoveryservices.](https://www.eurofinsdiscoveryservices.com/) 1083
[com/](https://www.eurofinsdiscoveryservices.com/), accessed May 23, 2018.
- 1084 (15) DiscoverX: <https://www.discoverx.com/home/>, 1085
accessed May 23, 2018.
- 1086 (16) Full details of the kinase profiling of **2** can be found in the 1087
[Supporting Information](#).

- 1088 (17) Heath, C. M.; Stahl, P. D.; Barbieri, M. A. Lipid Kinases Play
1089 Crucial and Multiple Roles in Membrane Trafficking and Signaling.
1090 *Histol. Histopathol.* **2003**, *18*, 989–998.
- 1091 (18) Heilmeyer, L. M. G., Jr.; Szivák, I.; Vereb, G.; Kakuk, A.; Vereb,
1092 G., Jr. Mammalian Phosphatidylinositol 4-Kinases. *IUBMB Life* **2003**,
1093 *55*, 59–65.
- 1094 (19) Balla, T. Phosphoinositides: Tiny Lipids With Giant Impact on
1095 Cell Regulation. *Physiol. Rev.* **2013**, *93*, 1019–1137.
- 1096 (20) Delang, L.; Paeshuyse, J.; Neyts, J. The Role of
1097 Phosphatidylinositol 4-Kinases and Phosphatidylinositol 4-Phosphate
1098 During Viral Replication. *Biochem. Pharmacol.* **2012**, *84*, 1400–1408.
- 1099 (21) McNamara, C. W.; Lee, M. C.; Lim, C. S.; Lim, S. H.; Roland,
1100 J.; Nagle, A.; Simon, O.; Yeung, B. K.; Chatterjee, A. K.; McCormack,
1101 S. L.; et al. Targeting Plasmodium PI(4)K to Eliminate Malaria.
1102 *Nature* **2013**, *504*, 248–253.
- 1103 (22) Boura, E.; Nencka, R. Phosphatidylinositol 4-Kinases: Function,
1104 Structure, and Inhibition. *Exp. Cell Res.* **2015**, *337*, 136–145.
- 1105 (23) Klima, M.; Toth, D. J.; Hexnerova, R.; Baumlova, A.;
1106 Chalupska, D.; Tykvar, J.; Rezabkova, L.; Sengupta, N.; Man, P.;
1107 Dubankova, A.; Humpolickova, J.; Nencka, R.; Veverka, V.; Balla, T.;
1108 Boura, E. Structural Insights and in Vitro Reconstitution of
1109 Membrane Targeting and Activation of Human PI4KB by the
1110 ACBD3 Protein. *Sci. Rep.* **2016**, *6*, 23641.
- 1111 (24) Sridhar, S.; Patel, B.; Aphkhasava, D.; Macian, F.;
1112 Santambrogio, L.; Shields, D.; Cuervo, A. M. The Lipid Kinase
1113 PI4KIIIbeta Preserves Lysosomal Identity. *EMBO J.* **2013**, *32*, 324–
1114 339.
- 1115 (25) Toth, B.; Balla, A.; Ma, H.; Knight, Z. A.; Shokat, K. M.; Balla,
1116 T. Phosphatidylinositol 4-Kinase IIIbeta Regulates the Transport of
1117 Ceramide Between the Endoplasmic Reticulum and Golgi. *J. Biol.*
1118 *Chem.* **2006**, *281*, 36369–36377.
- 1119 (26) Dornan, G. L.; McPhail, J. A.; Burke, J. E. Type III
1120 Phosphatidylinositol 4 Kinases: Structure, Function, Regulation,
1121 Signalling and Involvement in Disease. *Biochem. Soc. Trans.* **2016**,
1122 *44*, 260–266.
- 1123 (27) Klima, M.; Chalupska, D.; Rozycki, B.; Humpolickova, J.;
1124 Rezabkova, L.; Silhan, J.; Baumlova, A.; Dubankova, A.; Boura, E.
1125 Kobuviral Non-Structural 3A Proteins act as Molecular Harnesses to
1126 Hijack the Host ACBD3 Protein. *Structure (Oxford, U. K.)* **2017**, *25*,
1127 219–230.
- 1128 (28) McPhail, J. A.; Ottosen, E. H.; Jenkins, M. L.; Burke, J. E. The
1129 Molecular Basis of Aichi Virus 3A Protein Activation of
1130 Phosphatidylinositol 4 Kinase IIIbeta, PI4KB, Through ACBD3.
1131 *Structure (Oxford, U. K.)* **2017**, *25*, 121–131.
- 1132 (29) Dubankova, A.; Humpolickova, J.; Klima, M.; Boura, E.
1133 Negative Charge and Membrane-Tethered Viral 3B Cooperate to
1134 Recruit Viral RNA Dependent RNA Polymerase 3D (pol). *Sci. Rep.*
1135 **2017**, *7*, 17309.
- 1136 (30) Knight, Z. A.; Gonzalez, B.; Feldman, M. E.; Zunder, E. R.;
1137 Goldenberg, D. D.; Williams, O.; Loewith, R.; Stokoe, D.; Balla, A.;
1138 Toth, B.; Balla, T.; Weiss, W. A.; Williams, R. L.; Shokat, K. M. A
1139 Pharmacological Map of the PI3-K Family Defines a Role for
1140 p110alpha in Insulin Signaling. *Cell* **2006**, *125*, 733–747.
- 1141 (31) Fowler, M. L.; McPhail, J. A.; Jenkins, M. L.; Masson, G. R.;
1142 Rutaganira, F. U.; Shokat, K. M.; Williams, R. L.; Burke, J. E. Using
1143 Hydrogen Deuterium Exchange Mass Spectrometry to Engineer
1144 Optimized Constructs for Crystallization of Protein Complexes: Case
1145 Study of PI4KIIIbeta with Rab11. *Protein Sci.* **2016**, *25*, 826–839.
- 1146 (32) Burke, J. E.; Inglis, A. J.; Perisic, O.; Masson, G. R.;
1147 McLaughlin, S. H.; Rutaganira, F.; Shokat, K. M.; Williams, R. L.
1148 Structures of PI4KIIIbeta Complexes Show Simultaneous Recruit-
1149 ment of Rab11 and its Effectors. *Science (Washington, DC, U. S.)* **2014**,
1150 *344*, 1035–1038.
- 1151 (33) Rutaganira, F. U.; Fowler, M. L.; McPhail, J. A.; Gelman, M. A.;
1152 Nguyen, K.; Xiong, A.; Dornan, G. L.; Tavshanjian, B.; Glenn, J. S.;
1153 Shokat, K. M.; Burke, J. E. Design and Structural Characterization of
1154 Potent and Selective Inhibitors of Phosphatidylinositol 4-Kinase
1155 IIIbeta. *J. Med. Chem.* **2016**, *59*, 1830–1839.
- (34) Lamarche, M. J.; Borawski, J.; Bose, A.; Capacci-Daniel, C.;
Colvin, R.; Dennehy, M.; Ding, J.; Dobler, M.; Drumm, J.; Gauthier, L.
A.; Gao, J.; Jiang, X.; Lin, K.; McKeever, U.; Puyang, X.; Raman, P.;
Thohan, S.; Tommasi, R.; Wagner, K.; Xiong, X.; Zabawa, T.; Zhu, S.;
Wiedmann, B. Anti-hepatitis C Virus Activity and Toxicity of Type III
Phosphatidylinositol 4-Kinase Beta Inhibitors. *Antimicrob. Agents
Chemother.* **2012**, *56*, 5149–5156.
- (35) Keaney, E. P.; Connolly, M.; Dobler, M.; Karki, R.; Honda, A.;
Sokup, S.; Karur, S.; Britt, S.; Patnaik, A.; Raman, P.; Hamann, L. G.;
Wiedmann, B.; LaMarche, M. J. 2-Alkylloxazoles as Potent and
Selective PI4KIIIbeta Inhibitors Demonstrating Inhibition of HCV
Replication. *Bioorg. Med. Chem. Lett.* **2014**, *24*, 3714–3718.
- (36) Decor, A.; Grand-Maitre, C.; Hucke, O.; O'Meara, J.; Kuhn, C.;
Constantineau-Forget, L.; Brochu, C.; Malenfant, E.; Bertrand-
Laperle, M.; Bordeleau, J.; Ghire, C.; Pesant, M.; Fazel, G.; Gorys,
V.; Little, M.; Boucher, C.; Bordeleau, S.; Turcotte, P.; Guo, T.;
Garneau, M.; Spickler, C.; Gauthier, A. Design, Synthesis and
Biological Evaluation of Novel Aminothiazoles as Antiviral Com-
pounds Acting Against Human Rhinovirus. *Bioorg. Med. Chem. Lett.*
2013, *23*, 3841–3847.
- (37) Raubo, P.; Andrews, D. M.; McKelvie, J. C.; Robb, G. R.;
Smith, J. M.; Swarbrick, M. E.; Waring, M. J. Discovery of Potent,
Selective Small Molecule Inhibitors of Alpha-Subtype of type III
Phosphatidylinositol 4-Kinase (PI4KIIIalpha). *Bioorg. Med. Chem.*
Letts. **2015**, *25*, 3189–3193.
- (38) Waring, M. J.; Andrews, D. M.; Faulder, P. F.; Flemington, V.;
McKelvie, J. C.; Maman, S.; Preston, M.; Raubo, P.; Robb, G. R.;
Roberts, K.; Rowlinson, R.; Smith, J. M.; Swarbrick, M. E.; Treinies,
I.; Winter, J. J.; Wood, R. J. Potent, Selective Small Molecule
Inhibitors of Type III Phosphatidylinositol 4-Kinase Alpha but not
Beta Inhibit the Phosphatidylinositol Signaling Cascade and Cancer
Cell Proliferation. *Chem. Commun. (Cambridge, U. K.)* **2014**, *50*,
5388–5390.
- (39) Arita, M.; Kojima, H.; Nagano, T.; Okabe, T.; Wakita, T.;
Shimizu, H. Phosphatidylinositol 4-Kinase III Beta is a Target of
Enviroxime-Like Compounds for Antipoliiovirus Activity. *J. Virol.*
2011, *85*, 2364–2372.
- (40) Catalano, J. G.; Gaitonde, V.; Beesu, M.; Leivers, A. L.;
Shotwell, J. B. Phenoxide Leaving Group SNAr Strategy for the Facile
Preparation of 7-Amino-3-aryl Pyrazolo[1,5-a]pyrimidines from a 3-
Bromo-7-phenoxy pyrazolo[1,5-a]pyrimidine Intermediate. *Tetrahe-
dron Lett.* **2015**, *56*, 6077–6079.
- (41) Leivers, A. L. Chemical Optimization of Novel Inhibitor
Classes Selectively Targeting PI4KIIIβ: A Novel Host Lipid Kinase
Crucial for Enterovirus Replication. Presented at the 249th National
Meeting of the American Chemical Society, Denver, CO, March 25,
2015.
- (42) Mejdrova, I.; Chalupska, D.; Plackova, P.; Muller, C.; Sala, M.;
Klima, M.; Baumlova, A.; Hrebabecky, H.; Prochazkova, E.; Dejmek,
M.; Strunin, D.; Weber, J.; Lee, G.; Matousova, M.; Mertlikova-
Kaiserova, H.; Ziebuhr, J.; Birkus, G.; Boura, E.; Nencka, R. Rational
Design of Novel Highly Potent and Selective Phosphatidylinositol 4-
Kinase IIIbeta (PI4KB) Inhibitors as Broad-Spectrum Antiviral
Agents and Tools for Chemical Biology. *J. Med. Chem.* **2017**, *60*,
100–118.
- (43) Humpolickova, J.; Mejdrova, I.; Matousova, M.; Nencka, R.;
Boura, E. Fluorescent Inhibitors as Tools to Characterize Enzymes:
Case Study of the Lipid Kinase Phosphatidylinositol 4-Kinase IIIbeta
(PI4KB). *J. Med. Chem.* **2017**, *60*, 119–127.
- (44) Mejdrova, I.; Chalupska, D.; Kogler, M.; Sala, M.; Plackova, P.;
Baumlova, A.; Hrebabecky, H.; Prochazkova, E.; Dejmek, M.; Guillon,
R.; Strunin, D.; Weber, J.; Lee, G.; Birkus, G.; Mertlikova-Kaiserova,
H.; Boura, E.; Nencka, R. Highly Selective Phosphatidylinositol 4-
Kinase IIIbeta Inhibitors and Structural Insight into Their Mode of
Action. *J. Med. Chem.* **2015**, *58*, 3767–3793.
- (45) MacLeod, A. M.; Mitchell, D. R.; Palmer, N. J.; Van de Poel,
H.; Conrath, K.; Andrews, M.; Leyssen, P.; Neyts, J. Identification of a
Series of Compounds with Potent Antiviral Activity for the Treatment
of Enterovirus Infections. *ACS Med. Chem. Lett.* **2013**, *4*, 585–589.

- (46) Compound **5** has $IC_{50} = 42$ nM against PI4KIII β (UCB data). Further profiling revealed that **5** is inactive ($IC_{50} > 9$ μ M) against all other lipid kinases tested.³⁴
- (47) Compound **9** has $IC_{50} = 8$ nM against PI4KIII β , while **11** has $IC_{50} = 4$ nM (UCB data). Both compounds were reported as having >10 000 selectivity for PI4KIII β over all other lipid kinases.⁴¹
- (48) Roden, D. M. Drug-Induced Prolongation of the QT Interval. *N. Engl. J. Med.* **2004**, *350*, 1013–1022.
- (49) Wrighton, S. A.; Vandenbranden, M.; Stevens, J. C.; Shipley, L. A.; Ring, B. J.; Rettie, A. E.; Cashman, J. R. In Vitro Methods for Assessing Human Hepatic Drug Metabolism: Their use in Drug Development. *Drug Metab. Rev.* **1993**, *25*, 453–484.
- (50) For the 250 kinases tested at Invitrogen, see the [Supporting Information](#).
- (51) For the dose–response data of **13** and **22** against the 12 lipid kinases tested, see the [Supporting Information](#).
- (52) Braccini, L.; Cirao, E.; Campa, C. C.; Perino, A.; Longo, D. L.; Tibolla, G.; Pregolato, M.; Cao, Y.; Tassone, B.; Damilano, F.; Laffargue, M.; Calautti, E.; Falasca, M.; Norata, G. D.; Backer, J. M.; Hirsch, E. PI3K-C2gamma is a Rab5 Effector Selectively Controlling Endosomal Akt2 Activation Downstream of Insulin Signalling. *Nat. Commun.* **2015**, *6*, 7400.
- (53) Mountford, S. J.; Zheng, Z.; Sundaram, K.; Jennings, I. G.; Hamilton, J. R.; Thompson, P. E. Class II but not Second Class: Prospects for the Development of Class II PI3K Inhibitors. *ACS Med. Chem. Lett.* **2015**, *6*, 3–6.
- (54) Neumann, C. M.; Oughton, J. A.; Kerkvliet, N. I. Anti-CD3 Induced T-cell Activation in Vivo: Flow Cytometric Analysis of Dose-Responsive, Time-Dependent, and Cyclosporin A Sensitive Parameters of CD4+ and CD8+ Cells from the Draining Lymph Nodes of C57Bl/6 Mice. *Int. J. Immunopharmacol.* **1992**, *14*, 1295–1304.
- (55) Berek, C.; Griffiths, G. M.; Milstein, C. Molecular Events During Maturation of the Immune Response to Oxazolone. *Nature* **1985**, *316*, 412–418.
- (56) Vehicle-treated animals would normally reject an allograft within 7–10 days of surgery.
- (57) Ingulli, E. Mechanism of Cellular Rejection in Transplantation. *Pediatr. Nephrol. (Berlin)* **2010**, *25*, 61–74.
- (58) Strumberg, D. Preclinical and Clinical Development of the Oral Multikinase Inhibitor Sorafenib in Cancer Treatment. *Drugs Today* **2005**, *41*, 773–784.
- (59) Skipper, P. L.; Kim, M. Y.; Sun, H. L.; Wogan, G. N.; Tannenbaum, S. R. Monocyclic Aromatic Amines as Potential Human Carcinogens: Old is New Again. *Carcinogenesis* **2010**, *31*, 50–58.
- (60) Hodgman, M. J.; Garrard, A. R. A Review of Acetaminophen Poisoning. *Crit. Care Clin.* **2012**, *28*, 499–516.
- (61) A mini AMES test was conducted by Charles River up to a top concentration of 1667 μ g per plate. Some precipitation was observed at the highest two concentrations (500 and 1667 μ g). Three strains used were TA1537, TA98, and TA100 in the presence and absence of metabolic activation (\pm S9).
- (62) Thompson, D. C.; Josephy, P. D.; Chu, J. W.; Eling, T. E. Enhanced Mutagenicity of Anisidine Isomers in Bacterial Strains Containing Elevated N-acetyltransferase Activity. *Mutat. Res., Genet. Toxicol. Test.* **1992**, *279*, 83–89.
- (63) Both KCN and GSH trapping experiments were conducted in isolated human liver microsomes. For details, see the [Supporting Information](#).
- (64) Lovering, F.; Bikker, J.; Humblet, C. Escape From Flatland: Increasing Saturation as an Approach to Improving Clinical Success. *J. Med. Chem.* **2009**, *52*, 6752–6756.
- (65) Saal, C.; Peterit, A. C. Optimizing Solubility: Kinetic Versus Thermodynamic Solubility Temptations and Risks. *Eur. J. Pharm. Sci.* **2012**, *47*, 589–595.
- (66) Compound **44** was tested in the AMES MPF format against bacteria (*Salmonella typhimurium*) strains TA98, TA100, TA1535, TA1537, and *E. coli* (uvrA). After 2 days of incubation with and without metabolic activation up to the top concentration of 2000 μ M, 1293 no mutagenic effect was observed.
- (67) Both KCN and GSH trapping experiments were conducted in isolated human liver microsomes. For details, see the [Supporting Information](#).
- (68) 2-Methyl-4-methoxy aniline-HCl salt was tested in the AMES MPF format against bacteria (*Salmonella typhimurium*) strains TA98, TA100, and TA1537. After 2 days of incubation with and without metabolic activation up to the top concentration of 1000 μ M, no mutagenic effect was observed.
- (69) Selectivity ratios for PI4KIII β over the lipid kinase family for compound **44** were generated using IC_{50} data provided by Life Technologies. The IC_{50} against PI4KIII β measured at Life Technologies for **44** was 5 nM.
- (70) Proteros: <http://www.proteros.com/>, accessed May 23, 2018.
- (71) For a figure detailing the difference in the level of order/disorder of chain A and chain B, see the [Supporting Information](#).
- (72) Bloom, J. W.; Raju, R. K.; Wheeler, S. E. Physical Nature of Substituent Effects in XH/pi Interactions. *J. Chem. Theory Comput.* **2012**, *8*, 3167–3174.
- (73) (3R)-4-(6-Amino-1-methyl-pyrazolo[3,4-d]pyrimidin-4-yl)-N-(4-methoxy-2-methyl-phenyl)-3-methyl-piperazine-1-carboxamide was synthesized in an analogous fashion to **44** using commercial 2-(R)-methyl-4-(tert-butoxycarbonyl)piperazine. It was found to have $IC_{50} = 1$ μ M against PI4KIII β and 3 μ M in the HuMLR.
- (74) Groom, C. R.; Bruno, I. J.; Lightfoot, M. P.; Ward, S. C. The Cambridge Structural Database. *Acta Crystallogr., Sect. B: Struct. Sci., Cryst. Eng. Mater.* **2016**, *72*, 171–179.
- (75) Sadowski, J.; Gasteiger, J.; Klebe, G. Comparison of Automatic Three-Dimensional Model Builders Using 639 X-Ray Structures. *J. Chem. Inf. Model.* **1994**, *34*, 1000–1008.
- (76) Harder, E.; Damm, W.; Maple, J.; Wu, C.; Reboul, M.; Xiang, J. Y.; Wang, L.; Lupyán, D.; Dahlgren, M. K.; Knight, J. L.; Kaus, J. W.; Cerutti, D. S.; Krilov, G.; Jorgensen, W. L.; Abel, R.; Friesner, R. A. OPLS3: A Force Field Providing Broad Coverage of Drug-Like Small Molecules and Proteins. *J. Chem. Theory Comput.* **2016**, *12*, 281–296.
- (77) Friesner, R. A.; Banks, J. L.; Murphy, R. B.; Halgren, T. A.; Klicic, J. J.; Mainz, D. T.; Repasky, M. P.; Knoll, E. H.; Shelley, M.; Perry, J. K.; Shaw, D. E.; Francis, P.; Shenkin, P. S. Glide: A New Approach for Rapid, Accurate Docking and Scoring. I. Method and Assessment of Docking Accuracy. *J. Med. Chem.* **2004**, *47*, 1739–1749.
- (78) Devos, T.; Sprangers, B.; Lin, Y.; Li, S.; Yan, Y.; Landuyt, W.; Lenaerts, C.; Rutgeerts, O.; Goebels, J.; Bullens, D.; De Wolf-Peeters, C.; Mathieu, C.; Waer, M.; Billiau, A. D. Occurrence of Autoimmunity after Xenotransplantation in T-cell Deficient Mice Depends on the Thymus Transplant Technique. *Transplantation* **2008**, *85*, 640–644.
- (79) For a more detailed explanation of the protein production process to facilitate crystallography, see the [Supporting Information](#).
- (80) For details of the model used, see the [Supporting Information](#).
- (81) Murshudov, G. N.; Vagin, A. A.; Dodson, E. J. Refinement of Macromolecular Structures by the Maximum-Likelihood Method. *Acta Crystallogr., Sect. D: Biol. Crystallogr.* **1997**, *53*, 240–255.
- (82) Emsley, P.; Cowtan, K. Coot: Model-Building Tools for Molecular Graphics. *Acta Crystallogr., Sect. D: Biol. Crystallogr.* **2004**, *60*, 2126–2132.
- (83) Molecular Networks GmbH, Germany, and Altamira, LLC, USA.
- (84) Murshudov, G. N.; Skubak, P.; Lebedev, A. A.; Pannu, N. S.; Steiner, R. A.; Nicholls, R. A.; Winn, M. D.; Long, F.; Vagin, A. A. REFMAC5 for the Refinement of Macromolecular Crystal Structures. *Acta Crystallogr., Sect. D: Biol. Crystallogr.* **2011**, *67*, 355–367.